iScience

CellPress

Article

Cytoplasmic RNA Sensor Pathways and Nitazoxanide Broadly Inhibit Intracellular *Mycobacterium tuberculosis* Growth

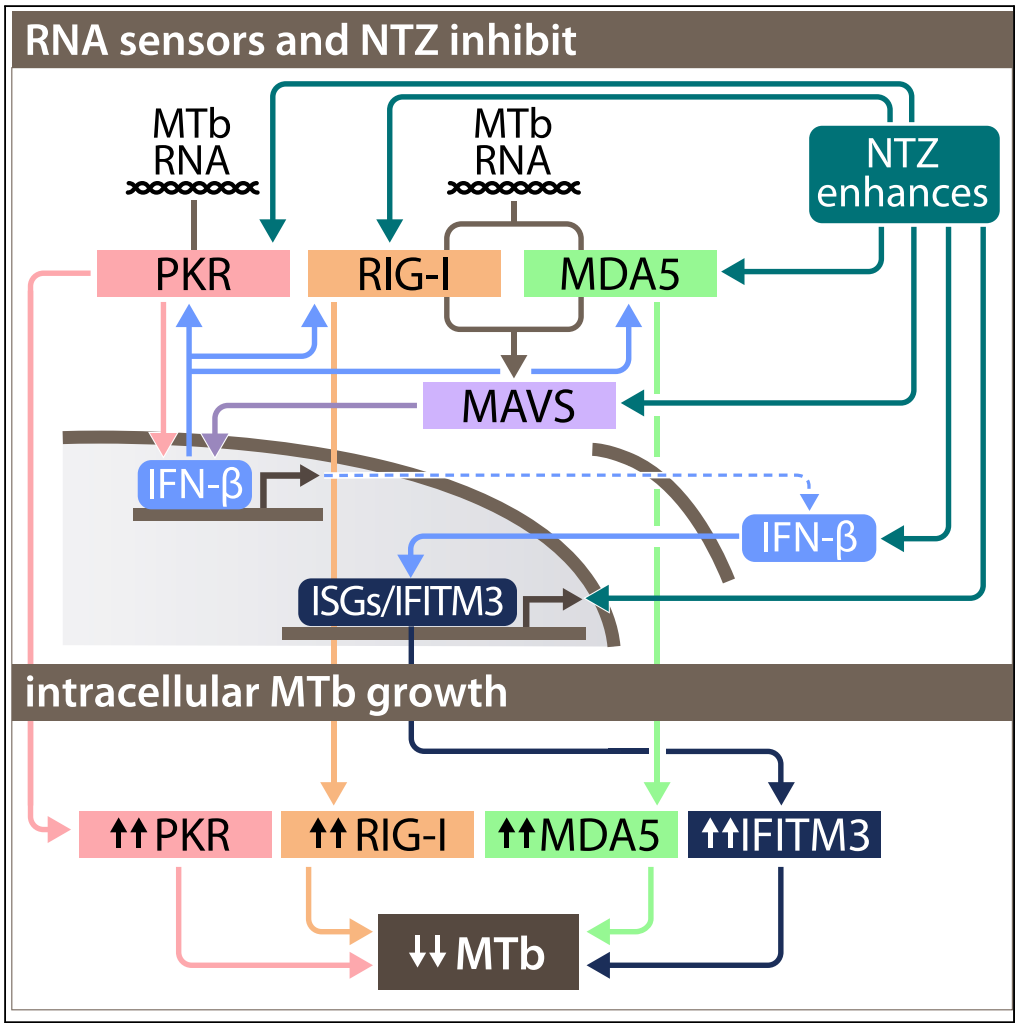

Shahin Ranjbar, Viraga Haridas, Aya Nambu, ..., Gail H. Cassell, James V. Falvo, Anne E. Goldfeld

anne.goldfeld@childrens.harvard.edu

HIGHLIGHTS

MTb infection induces RNA sensor (RIG-I, MDA5, PKR) mRNA levels and activities

RIG-I, MDA5, MAVS, and PKR restrict intracellular MTb growth in human cells

NTZ enhances MTb-driven RNA sensor mRNA levels and RLR activities

NTZ and NTZ derivatives inhibit intracellular MTb growth in primary human cells

Ranjbar et al., iScience 22, 299–313
December 20, 2019
https://doi.org/10.1016/j.isci.2019.11.001

iScience

CellPress

Article

Cytoplasmic RNA Sensor Pathways and Nitazoxanide Broadly Inhibit Intracellular *Mycobacterium tuberculosis* Growth

Shahin Ranjbar,[1,5] Viraga Haridas,[1,5] Aya Nambu,[1] Luke D. Jasenosky,[1,4] Supriya Sadhukhan,[1] Thomas S. Ebert,[2] Veit Hornung,[2] Gail H. Cassell,[3] James V. Falvo,[1] and Anne E. Goldfeld[1,6,*]

SUMMARY

To establish stable infection, *Mycobacterium tuberculosis* (MTb) must overcome host innate immune mechanisms, including those that sense pathogen-derived nucleic acids. Here, we show that the host cytosolic RNA sensing molecules RIG-I-like receptor (RLR) signaling proteins RIG-I and MDA5, their common adaptor protein MAVS, and the RNA-dependent kinase PKR each independently inhibit MTb growth in human cells. Furthermore, we show that MTb broadly stimulates RIG-I, MDA5, MAVS, and PKR gene expression and their biological activities. We also show that the oral FDA-approved drug nitazoxanide (NTZ) significantly inhibits intracellular MTb growth and amplifies MTb-stimulated RNA sensor gene expression and activity. This study establishes prototypic cytoplasmic RNA sensors as innate restriction factors for MTb growth in human cells and it shows that targeting this pathway is a potential host-directed approach to treat tuberculosis disease.

INTRODUCTION

Type I interferons (IFNs), including IFN-β, play a central role in MTb restriction and pathogenesis (Kaufmann and Dorhoi, 2013; Moreira-Teixeira et al., 2018; Pandey et al., 2014). Our previous studies unexpectedly showed that the virus- and IFN-inducible interferon-stimulated gene (ISG) IFITM3 was induced by MTb in primary human monocyte-derived macrophages (MDM) and was critically involved in MTb growth inhibition in human monocytic and alveolar epithelial cell lines (Ranjbar et al., 2015). These findings led us to speculate that mycobacteria directly trigger cytosolic RNA sensors that lead to transcription of IFN-β and of IFITM3 and other ISGs typically involved in the antiviral/IFN axis, which might also inhibit intracellular MTb growth in human cells.

Activation of cytosolic DNA sensing pathways by MTb infection leading to type I IFN production was first described in 2012 (Manzanillo et al., 2012), followed by observations from several laboratories that the cyclic GMP-AMP synthase (cGAS)/stimulator of interferon genes (STING)/TANK binding kinase 1 (TBK1)/IFN regulatory factor 3 (IRF3) pathway was important for MTb-dependent type I IFN production (Collins et al., 2015; Dey et al., 2015; Wassermann et al., 2015; Watson et al., 2015). STING and cGAS were also shown to restrict MTb growth with the demonstration that bone-marrow-derived macrophages (BMDMs) from cGAS$^{-/-}$ and STING$^{-/-}$ mice had a higher burden of MTb relative to BMDM from wild-type mice (Watson et al., 2015).

The RLR proteins retinoid acid-inducible gene I (RIG-I) and melanoma differentiation-associated protein 5 (MDA5) are key components of the host cytosolic RNA sensing pathway (Cui et al., 2014; Wu and Hur, 2015). Although RIG-I and MDA5 each preferentially respond to distinct double-stranded RNA (dsRNA) ligands—short polyphosphorylated dsRNA (RIG-I) and long dsRNA (MDA5)—both signal through a common adaptor, the mitochondrial antiviral signaling (MAVS) protein, leading to expression of IFN-β and other type I IFNs (Gebhardt et al., 2017; Reikine et al., 2014; Tatematsu et al., 2018). The IFN-inducible, cytoplasmic dsRNA-activated kinase protein kinase R (PKR), which is an RNA-sensing protein outside of the RIG-I/MDA5/MAVS axis, is also triggered by viral infection and by natural or synthetic dsRNA (Bou-Nader et al., 2019; Dalet et al., 2015; Gal-Ben-Ari et al., 2018; Hull and Bevilacqua, 2016; Munir and Berg, 2013).

A role for cytosolic RNA sensing via the RLR pathway in response to bacterial infection has emerged from studies in murine cells. In murine macrophages RIG-I and MDA5 have been shown to recognize RNA

[1]Program in Cellular and Molecular Medicine, Children's Hospital Boston, Harvard Medical School, Boston, MA 02115, USA

[2]Gene Center and Department of Biochemistry, Ludwig-Maximilians-Universität München, Munich, Germany

[3]Department of Global Health and Social Medicine, Harvard Medical School, Boston, MA 02115, USA

[4]Present address: Profectus Biosciences, Pearl River, NY 10965, USA

[5]These authors contributed equally

[6]Lead Contact

*Correspondence: anne.goldfeld@childrens.harvard.edu

https://doi.org/10.1016/j.isci.2019.11.001

released by *Legionella pneumophila* (Monroe et al., 2009) and *Listeria monocytogenes* (Abdullah et al., 2012), and RIG-I has been shown to recognize *Helicobacter pylori* RNA in murine dendritic cells (Rad et al., 2009). Furthermore, MTb infection of murine BMDM and J774 cells resulted in increased RIG-I and MDA5 mRNA levels (Andreu et al., 2017), and MTb RNA actively released into the host cytoplasm has been shown to interact with RIG-I (Cheng and Schorey, 2018).

Here, we show that the RNA sensors RIG-I, MDA5, MAVS, and PKR broadly inhibit MTb growth in human cells. Furthermore, we show that MTb stimulates RLR and PKR functional activity. We also demonstrate that the oral FDA-approved thiazolide drug nitazoxanide (NTZ) (Anderson and Curran, 2007; Rossignol, 2014), which we have recently shown to amplify RNA sensing and interferon pathways in response to virus and double-stranded RNA (dsRNA) (Jasenosky et al., 2019), potentiates MTb-driven RLR activity and significantly inhibits intracellular MTb growth in primary human cells. This study presents the first evidence of the involvement of the RLR/MAVS and PKR pathways in cell-intrinsic control of intracellular MTb growth, demonstrates the broad role of cytosolic RNA sensing proteins in the type I IFN response to MTb in human cells, and suggests this pathway as a potential target for host-directed approaches to treat tuberculosis disease.

RESULTS

MTb Infection Induces Expression of RIG-I, MDA5, and PKR mRNA in Primary Human MDM and THP-1 Cells

IFITM3, RIG-I, MDA5, and PKR are IFN-stimulated genes (ISGs) (Katze et al., 1991; Kawasaki and Kawai, 2019; Meurs et al., 1990), whereas MAVS has not been reported to be IFN inducible (Kawasaki and Kawai, 2019). To determine if, as is the case with IFN-inducible IFITM3 (Ranjbar et al., 2015), RIG-I, MDA5, PKR, and/or MAVS gene expression is induced by MTb in human cells, we infected primary human MDM for 3 or 24 h with MTb strain H37Rv. By 24 h post-MTb infection, RIG-I, MDA5, and PKR mRNA levels significantly increased ($p < 0.0001$), whereas constitutive MAVS gene expression was not further elevated (Figure 1A, left). We also examined IFN-β gene expression after 3 and 24 h of MTb infection and found that it too was highly induced at 24 h (p=<0.000.1), and minimally, but significantly, induced by MTb at 3 h post-infection ($p = 0.01$) (Figure 1A, left).

We have previously used human monocytic THP-1 cells to study MTb-induced human gene transcription and the role of host factors in restriction of MTb (Barthel et al., 2003; Ranjbar et al., 2012, 2015), including IFITM3 (Ranjbar et al., 2015). In a pattern similar to MDM, after 24 h of H37Rv MTb infection of THP-1 cells, mRNA levels of RIG-I ($p = 0.002$), MDA5 ($p = 0.0001$), and PKR ($p = 0.006$) were significantly increased, whereas MAVS mRNA levels were not (Figure 1A, right). This is consistent with a recent study showing an increase in MDA5 and PKR mRNA levels in MTb-infected human MDM and THP-1 cells (Zhou et al., 2019). MTb infection of THP-1 cells also led to a significant increase in IFN-β mRNA levels after 24 h (<0.0001) (Figure 1A, right) as found in MDM. Thus, MTb infection stimulates RIG-I, MDA5, and PKR gene expression in both primary human MDM and THP-1 cells.

To examine if this was a consequence of live MTb infection, we also tested the ability of killed mycobacterial extracts to induce RIG-I, MDA5, and PKR mRNA levels. Treatment of THP-1 cells with MTb H37Rv whole-cell lysates for 24 h significantly induced RIG-I, MDA5, and PKR mRNA levels with no increase in MAVS mRNA levels in a pattern very similar to live infection (Figure S1A). Furthermore, IFITM3 mRNA levels were also induced by the MTb lysates (Figure S1A). This result is consistent with our previous study showing that IFITM1-3 gene expression was induced by engagement of the pattern recognition receptors (PRRs) toll-like receptor 2 (TLR2) and TLR4 (Ranjbar et al., 2015), which recognize MTb-derived molecules (Falvo et al., 2011).

Disruption of Specific Cytoplasmic RNA Sensor Proteins Promotes Increased Intracellular MTb Growth in Human Cells

Having established that MTb infection induces gene expression of the RLR proteins and PKR, we next tested the effect of disrupting expression of RIG-I, MDA5, MAVS, or PKR (Figure S1B) upon intracellular MTb growth compared with its respective control THP-1 cell line. However, first we performed a control experiment to establish the RNA and DNA sensor responsiveness of the cell lines where the RNA sensor proteins had been perturbed. We stimulated each knockdown and control cell line with short (19-bp) dsRNA (5′ppp dsRNA) and long (~1.5–8 kb) dsRNA (poly I:C) ligands and with herring sperm DNA, a ligand stimulating the DNA sensing pathway, and measured IFN-β mRNA induction. We note that RIG-I

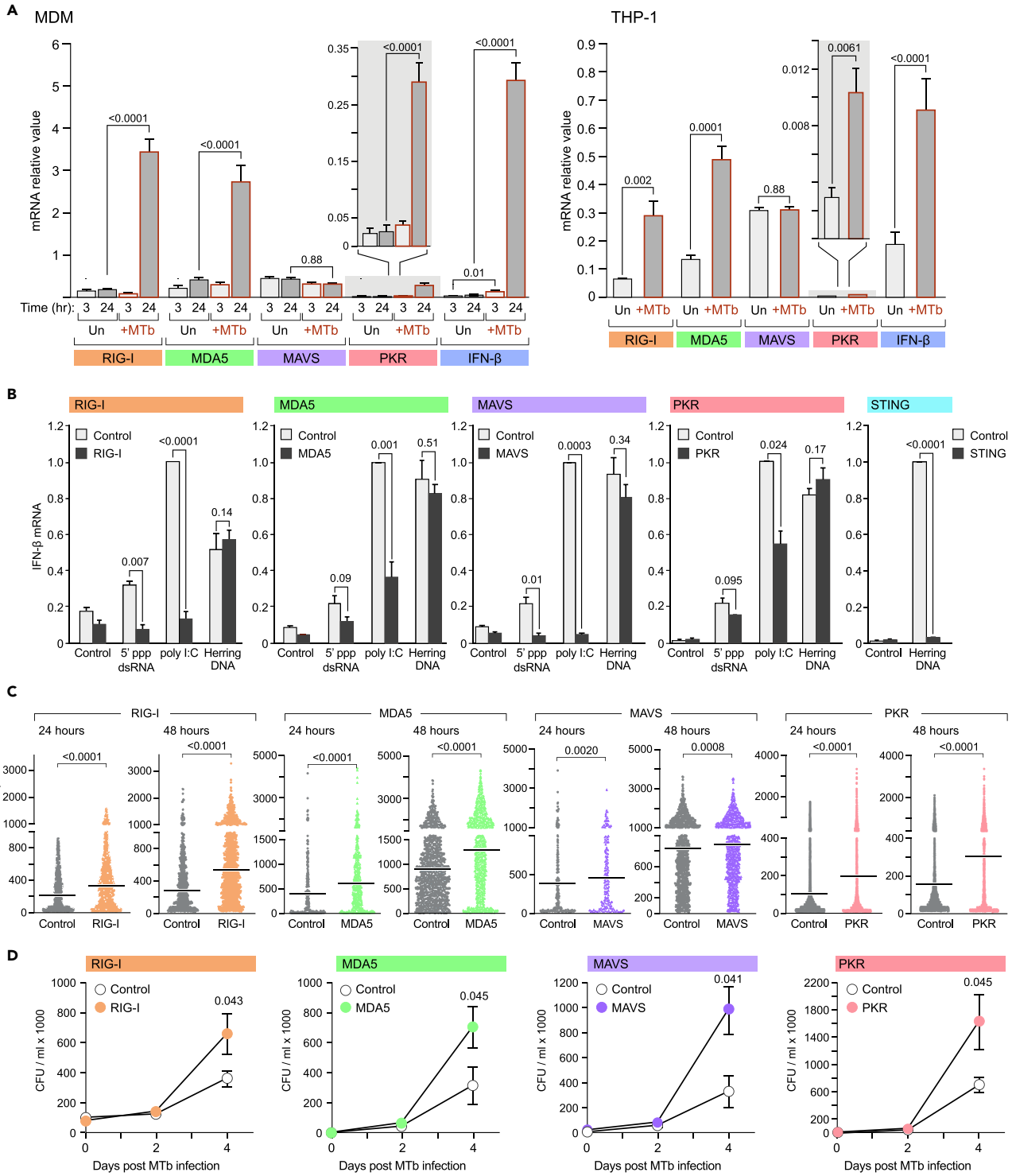

Figure 1. MTb Infection Induces Gene Expression of Cytosolic RNA Sensing Proteins, Which Inhibit MTb Growth

(A) Gene expression in MDM (left) or THP-1 cells (right) that were mock-infected or infected with MTb (H37Rv) at ratio of 1:10 cell:bacilli for 3 or 24 h (MDM) or 24 h (THP-1). Relative mRNA expression of RIG-I, MDA5, MAVS, PKR, or IFN-β measured by RT-PCR is indicated on the histogram. Data were analyzed using the unpaired Student's t-test and are presented as mean ± SEM of three independent experiments. Please see Figure S1A for RNA analysis of RIG-I, MDA5, MAVS, PKR, and IFITM3 after H37Rv extract stimulation of THP-1 cells.

Figure 1. *Continued*

(B) Knockdown of RIG-I by shRNA, MDA5 or MAVS by Cas9/CRISPR, or PKR by dCas9/CRISPR in THP-1 cells as described in Methods impairs the cytosolic RNA sensing pathway while leaving the cytosolic DNA sensing pathway intact. IFN-β mRNA expression levels were measured in the differentiated THP-1 control cells or RIG-I, MDA5, MAVS, PKR, or STING knockdown cells. THP-1 cells were treated with 5′ppp RNA, poly I:C, or herring sperm DNA as indicated for eight hours. For each THP-1 cell line with an RNA sensor disruption we paired a matched control THP-1 cell line. In the case of the MDA5, MAVS, or STING disrupted cells, which were created by Cas9/CRISPR, we employed a WT THP-1 cell line that was parental to the specific Cas9/CRISPR clone as described previously (Mankan et al., 2014; Paijo et al., 2016; Schmid-Burgk et al., 2014). In the case of the RIG-I disrupted cells, we used an shRNA control THP-1 cell line generated at the same time, and in the case of the PKR disrupted cells, which were generated by dCas9, we used a dCas9 control cell line as described in Methods. Data were analyzed using the unpaired Student's t-test and are presented as mean ± SEM of three independent experiments. Please see Figure S1B for Western blot analyses showing ablation of protein expression of RIG-I, MDA5, MAVS, and PKR in THP-1 cells where expression of these genes have been disrupted.

(C) Quantitative IFC analysis of THP-1 cells infected with H37Rv-mCherry at 1:10 cell:bacilli for 24 h or 48 h, comparing THP-1 control cells with cells in which RIG-I, MDA5, MAVS, or PKR expression was ablated as described in Methods. Dot plot graphs show the pixel intensity of intracellular mCherry in the infected cells after ImageStream acquisition. Data were analyzed using the Mann-Whitney Test and are representative of three independent experiments, acquiring ~5,000 cells per sample each time. Please see Figure S2 for increase of MTb growth in STING- or cGAS-deficient THP-1 cells, and, please refer to Figure S3 for representative images of sensor-deficient and control THP-1 cells after ImageStream acquisition.

(D) CFU assays at 0, 2, and 4 days post-MTb infection (1:10 cell:bacilli) of control THP-1 cells relative to THP-1 cells in which RIG-I, MDA5, MAVS, or PKR expression was ablated as indicated. At Day 0, the range of counts were as follows: RIG-I vs. control: $72 \times 10^3 \pm 22$ vs. $92 \times 10^3 \pm 1$; MDA5 vs. control: $17 \times 10^3 \pm 8$ vs. $6 \times 10^3 \pm 3$; MAVS vs. control: $18.1 \times 10^3 \pm 8$ vs. $6.3 \times 10^3 \pm 3$; PKR vs. control: $13 \times 10^3 \pm 1.1$ vs. $9 \times 10^3 \pm 1.9$. Data were analyzed using the unpaired Student's t-test and are presented as mean ± SEM of two independent experiments in triplicate.

preferentially interacts with shorter dsRNAs compared with MDA5 and PKR, which preferentially respond to longer dsRNAs (Gebhardt et al., 2017; Kato et al., 2008; Reikine et al., 2014; Tatematsu et al., 2018).

In response to 5′ppp dsRNA, the RIG-I-deficient cells displayed significantly decreased expression of IFN-β mRNA ($p = 0.007$) compared with control cells, which is consistent with RIG-I's preference for shorter dsRNAs (Gebhardt et al., 2017; Reikine et al., 2014; Tatematsu et al., 2018). By contrast, 5′ppp dsRNA stimulation of the MDA5-and PKR-deficient THP-1 cells did not result in significantly decreased ($p = 0.09$ and $p = 0.095$, respectively) IFN-β levels compared with control cells (Figure 1B). These results are consistent with the preferential response of MDA5 and PKR to longer dsRNAs (Gebhardt et al., 2017; Reikine et al., 2014; Tatematsu et al., 2018). Consistent with this finding, in response to poly I:C, the MDA5- or PKR-deficient cells displayed significantly decreased IFN-β expression ($p = 0.001$ and $p = 0.024$, respectively) compared with their respective controls (Figure 1B). As expected, cells deficient in MAVS, through which both RIG-I and MDA5 signal, displayed a significant decrease in IFN-β mRNA levels in response to both 5′ppp dsRNA ($p = 0.01$) and poly I:C ($p = 0.003$) compared with their control THP-1 cells (Figure 1B).

Because there is potential crosstalk between the cytoplasmic DNA and RNA sensing pathways (Zevini et al., 2017), to rule out an impact of disruption of the RNA sensors upon DNA sensing activities we stimulated the RIG-I-, MDA5-, MAVS-, and PKR-deficient cell lines with herring sperm DNA (hsDNA), which activates the cGAS/STING pathway (Gaidt et al., 2017). All of the RNA sensor-deficient cell lines displayed IFN-β gene expression levels equivalent to those of control cells in response to hsDNA (Figure 1B). As a control, we also stimulated STING-deficient THP-1 cells (Figure S1B), which as expected did not respond to hsDNA as did its control THP-1 cell line (Figure 1B). Taken together, these data show that our RNA sensor-deficient cell lines displayed functional phenotypes reflecting the lack of the specific sensor that was targeted, and their DNA sensing pathway was intact.

To determine the role of each specific sensor in the cell-intrinsic inhibition of intracellular MTb growth, we next infected the RIG-I, MDA5, MAVS, or PKR-deficient THP-1 cell lines with fluorescently labeled H37Rv-mCherry MTb (Sillé et al., 2011) at a cell to bacteria ratio of 1:10 and compared their ability to restrict MTb growth as compared to their respective control THP-1 cells. MTb growth was then evaluated after 24 or 48 h by quantitative imaging flow cytometry (IFC) (Figure 1C) utilizing the ImageStream platform (Basiji et al., 2007; Haridas et al., 2017; Ranjbar et al., 2015). IFC permits discernment of internalized MTb bacilli from extracellular bacilli within acquired images, and thus data are generated in a high-throughput fashion from image analysis of specific cellular parameters (Haridas et al., 2017; Ranjbar et al., 2015). Intensity of intracellular fluorescence per cell can then be plotted as a graph of pixel intensity (Basiji et al., 2007; Doan et al., 2018; Haridas et al., 2017).

As shown in Figure 1C, inhibition of each of the RNA sensors resulted in highly significant increased growth of H37Rv-mCherry as detected by IFC/ImageStream relative to its control cell line at 24 h (RIG-I: $p < 0.0001$;

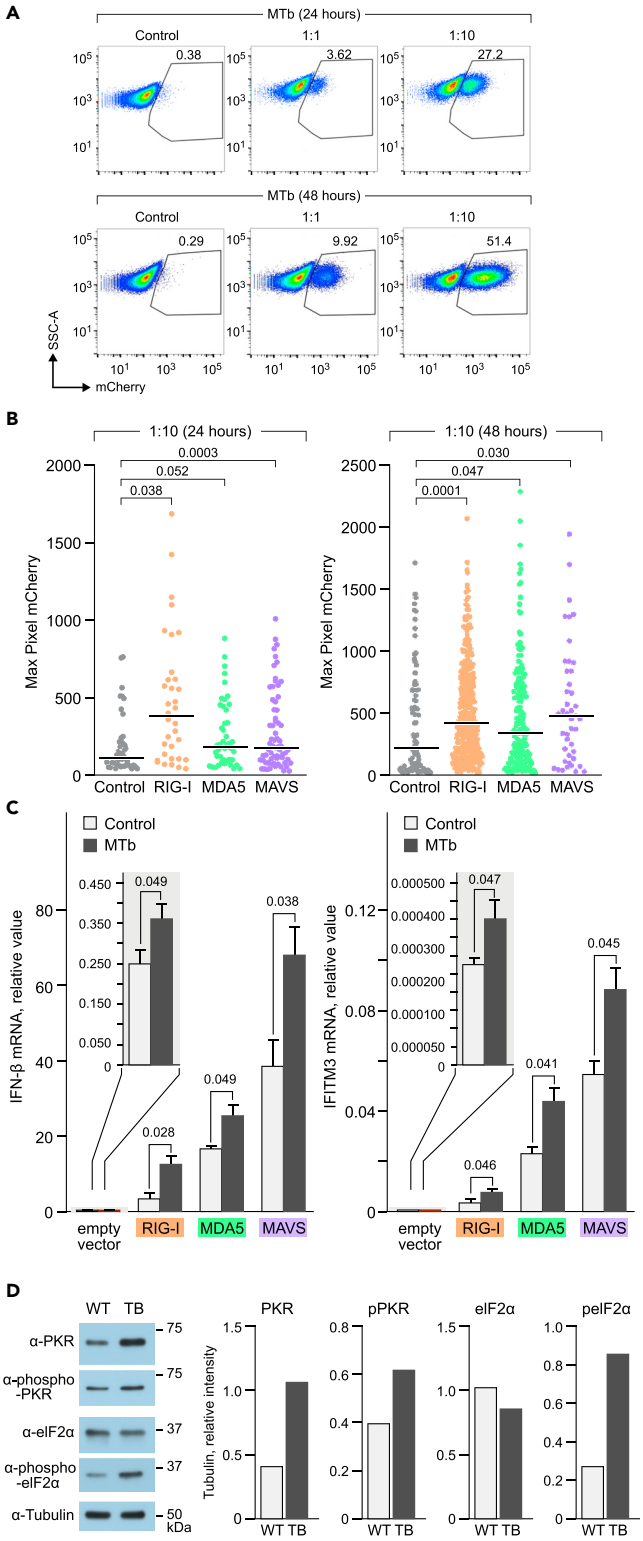

Figure 2. MTb Enhances RLR and PKR Activities

(A) 293T cells were left uninfected or infected with MTb strain H37Rv-mCherry (1:1 or 1:10 cell:bacilli) for 24 h (top row) or 48 h (bottom row) and analyzed by flow cytometry. Gated area and numerical values show the percentage of the cells infected with bacilli. Dot plots are representative of three independent experiments.

Figure 2. *Continued*

(B) ImageStream quantitative IFC analysis of 293T cells infected with H37Rv-mCherry at 1:10 cell:bacilli for 24 h (left) or 48 h (right) comparing WT 293T control cells with cells in which RIG-I, MDA5, or MAVS expression was disrupted by gene editing as described in Methods. A control 293T cell line that was parental to the specific gene-edited clone was used as described previously (Ablasser et al., 2013; Yao et al., 2015; Zhu et al., 2014). Data were analyzed using the Mann-Whitney Test and are representative of three independent experiments acquiring ~5,000 cells per sample each time. Please see Figure S1C for Western blot analysis showing ablation of protein expression of RIG-I, MDA5, and MAVS, in 293T cells where expression of these genes have been disrupted.

(C) IFN-β mRNA expression (left panel) and IFITM3 mRNA expression (right panel) in 293T cells transfected with human RIG-I, MDA5, or MAVS expression vector or empty vector control in uninfected cells or cells infected with MTb (1:10 cell:bacilli) for 24 h. Data were analyzed using the unpaired Student's t-test and are presented as mean ± SEM of three independent experiments.

(D) Left: Western blot analysis of total PKR and eIF2α, and phosphorylated PKR and eIF2α, and tubulin from control and MTb (H37Rv)-infected (24 h) THP-1 cells. Right: densitometric analysis of the data is presented in histogram format. Please see Figure S4 for Western blot analysis of RIG-I, MDA5, and MAVS protein levels in THP-1 cells after MTb (H37Rv) infection.

MDA5: $p < 0.0001$; MAVS: $p = 0.002$) or 48 h (RIG-I: $p < 0.0001$; MDA5: $p < 0.0001$; MAVS: $p = 0.0008$) post-infection. We also infected THP-1 cells in which STING or cGAS expression was ablated. Consistent with previous results in murine cGAS$^{-/-}$ and STING$^{-/-}$ BMDM (Watson et al., 2015), infection with H37Rv-mCherry resulted in significantly enhanced growth of MTb at 24 or 48 h post-infection relative to control cells (Figure S2), which was comparable to that observed with disruption of individual RNA sensor proteins. Representative images of intracellular mycobacteria from the IFC/ImageStream analysis at the median fluorescence intensity level for each mutant cell line and its corresponding control cell line are shown in Figure S3.

We next confirmed our findings in an independent classical colony-forming unit (CFU) analysis. Inhibition of RIG-I ($p = 0.043$), MDA5 ($p = 0.045$), MAVS ($p = 0.041$), and PKR ($p = 0.045$) each resulted in significant increase of MTb growth in comparison to THP-1 control cells by CFU analysis (Figure 1D). We note that there was no significant difference in numbers of bacteria between any of the cell lines with RNA sensor disruptions compared with their control cell lines at Day 0 after 4 h of MTb growth or at Day 2. Taken together, we conclude that the RLR and PKR RNA sensing pathways broadly inhibit MTb intracellular growth independently of the cGAS/STING DNA sensing pathway.

RIG-I, MDA5, and MAVS Activities Are Potentiated by MTb Infection and PKR Is Activated

We next sought to determine if MTb, in addition to inducing gene expression of cytoplasmic RNA sensors, amplified their activities. Previous studies of RLR activation have employed human embryonic kidney (HEK) 293T cells to overexpress RLRs and to test their response to specific activators (Ahmad et al., 2018; Jasenosky et al., 2019; Wu et al., 2013, 2014). To determine if 293T cells were an appropriate model system to evaluate MTb-stimulated RLR activities, we first established that MTb could infect these cells. We note that although MTb can proliferate in renal cells (Daher Ede et al., 2013), 293T cells are not a typical cell line in which to study MTb infection. As shown in Figure 2A, H37Rv-mCherry MTb infection and growth in 293T cells were detectable by flow cytometry when cells were infected with bacteria at a ratio of 1:1 or 1:10 after 24 (Figure 2A, top row) or 48 h (Figure 2A, bottom row).

Given the infectability of 293T cells by MTb, we next examined whether endogenous RIG-I, MDA5, or MAVS within 293T cells played a role in restriction of H37Rv MTb growth in these cells. Infection of CRISPR/Cas9 gene-edited 293T cells in which RIG-I, MDA5, or MAVS expression was ablated (Figure S1C) resulted in significant increase of intracellular growth of MTb relative to control 293T cells evaluated by IFC (Figure 2B). Thus, MTb infection of 293T cells is restricted by RLR proteins, which mirrored our findings of their role in the monocytic THP-1 cells (Figure 1C).

We thus next overexpressed RIG-I, MDA5, or MAVS in 293T cells and infected the cells with MTb H37Rv at a ratio of 1:10 (Figure 2C). Twenty-four hours later we measured IFN-β (Figure 2C, left panel) and IFITM3 (Figure 2C, right panel) mRNA levels. Expression of both IFN-β and IFITM3 was significantly enhanced by MTb infection in comparison to overexpression of each RNA sensor in the absence of MTb infection (Figure 2C). Thus, MTb amplifies the activity of RIG-I and MDA5 and their signaling adaptor protein MAVS, resulting in increased levels of IFN-β and IFITM3 mRNA.

Activation of PKR can be measured by detection of its auto-phosphorylated form (Carroll et al., 1993; Galabru and Hovanessian, 1987; Thomis and Samuel, 1993) and by phosphorylation of its substrate eIF2α (Bou-Nader et al., 2019; Dalet et al., 2015; Gal-Ben-Ari et al., 2018; Hull and Bevilacqua, 2016; Munir and Berg, 2013). To test if MTb activated PKR, we infected THP-1 cells with H37Rv MTb for 24 h, prepared cellular extracts, and performed a Western blot analysis. We observed higher levels of total PKR protein and its phosphorylated active form and higher levels of phosphorylated eIF2α protein after MTb infection (Figure 2D). Thus, MTb infection enhances PKR activity in THP-1 cells as evidenced by the increased phosphorylation of eIF2α. We note that the MTb-induced protein expression of RIG-I, MDA5, and MAVS (Figure S4) was also directly correlated with their RNA expression shown in Figure 1A.

NTZ Enhances MTb-Induced Gene Expression and Activity

Our recent studies have shown that the FDA-approved small molecule drug, NTZ, enhances RLR and PKR activity in human cells (Jasenosky et al., 2019). Given our results above, we tested its effect on MTb-driven RIG-I, MDA5, MAVS, and PKR gene expression in THP-1 cells. THP-1 cells were exposed to vehicle (DMSO) or 10 μM NTZ for 4 h and then infected with MTb. As shown in Figure 3A, NTZ augmented MTb induction of RIG-I ($p = 0.04$), MDA5 ($p = 0.03$), PKR ($p = 0.01$), and MAVS ($p = 0.06$) mRNA levels.

To test whether NTZ amplified MTb-driven RLR activities in 293T cells overexpressing RIG-I, MDA5, or MAVS, we next examined the impact of treatment of the cells with 10 μM NTZ for 4 h prior to MTb infection. As shown in Figure 3B, NTZ pretreatment significantly increased MTb-induced IFN-β and IFITM3 gene expression in cells overexpressing RIG-I ($p = 0.02$; $p = 0.02$), MDA5 ($p = 0.01$, $p = 0.01$), or MAVS ($p = 0.01$; $p = 0.004$), respectively. Previous studies (Ashiru et al., 2014; Elazar et al., 2009) have suggested that phosphorylation of PKR is increased by NTZ treatment. We thus also evaluated levels of PKR or phosphorylated PKR in cellular extracts from THP-1 cells stimulated with 10 μM NTZ or vehicle for 4 h and then infected with MTb H37Rv for 24 h. We did not observe an NTZ-dependent increase in PKR phosphorylation in these cells (Figure S4), consistent with a recent report (Hickson et al., 2018). Thus, NTZ broadly enhanced MTb-induced RIG-I, MDA5, and PKR mRNA expression and amplified MTb-dependent activation of the RLR proteins.

Inhibition of MTb Growth by NTZ

NTZ has been reported to inhibit the growth of diverse strains of MTb cultured in cell-free media (Cavanaugh et al., 2017; de Carvalho et al., 2009, 2011; Harausz et al., 2016; Odingo et al., 2017; Piccaro et al., 2013; Shigyo et al., 2013). In one study using an H37Rv-luciferase reporter MTb strain, NTZ inhibited MTb replication in THP-1 cells when measured at 24, 48, and 72 h after infection (Lam et al., 2012). By contrast, in another study utilizing a whole blood assay (WBA) (Wallis et al., 2003) of human donor cells and H37Rv, a significant inhibitory effect of NTZ was not appreciated, which the authors suggested was due to low bioavailability of the highly protein-bound drug (Harausz et al., 2016). We note that another WBA-based study did not show an inhibitory effect upon MTb of orally administered clofazimine (Janulionis et al., 2004), which, as is the case with NTZ, is also highly protein-bound (Sangana et al., 2018), even though clofazimine is now effectively used as a therapy for drug-resistant TB that is refractory to second-line agents (Hurtado et al., 2018).

To test NTZ's effect on MTb growth, we first treated THP-1 cells with 5 or 10 μM NTZ (or vehicle) 4 h before or 4 h after infection with H37Rv-mCherry at cell to bacteria ratios of 1:1 and 1:10 and evaluated MTb growth 24 or 48 h post-infection by FACS. NTZ-dependent inhibition of MTb growth was evident when NTZ (5 or 10 μM) was added 4 h prior to MTb infection but not when it was added 4 h after infection irrespective of cell to bacteria ratio (Figure 4A).

To further quantify this effect, we evaluated NTZ's impact by IFC and the ImageStream platform. As shown in Figure 4B, when 5 or 10 μM NTZ was added 4 h prior to H37Rv-mCherry infection of THP-1 cells, there was a highly significant inhibitory effect on MTb growth at both 24 ($p = 0.008$, $p < 0.0001$) and 48 h ($p < 0.0001$, $p < 0.0001$). By contrast, when 5 or 10 μM NTZ was added 4 h after infection, no MTb inhibition was observed at 24 ($p = 0.28$, $p = 0.63$) or 48 h ($p = 0.46$, $p = 0.11$). Our data indicate that detection of NTZ's host-dependent effects is maximized by pretreatment of cells with NTZ prior to infection.

To confirm our findings showing NTZ inhibition of MTb growth by FACS and IFC, we next performed a third independent analysis of NTZ's impact on MTb growth by quantifying CFUs using the H37Rv MTb strain and

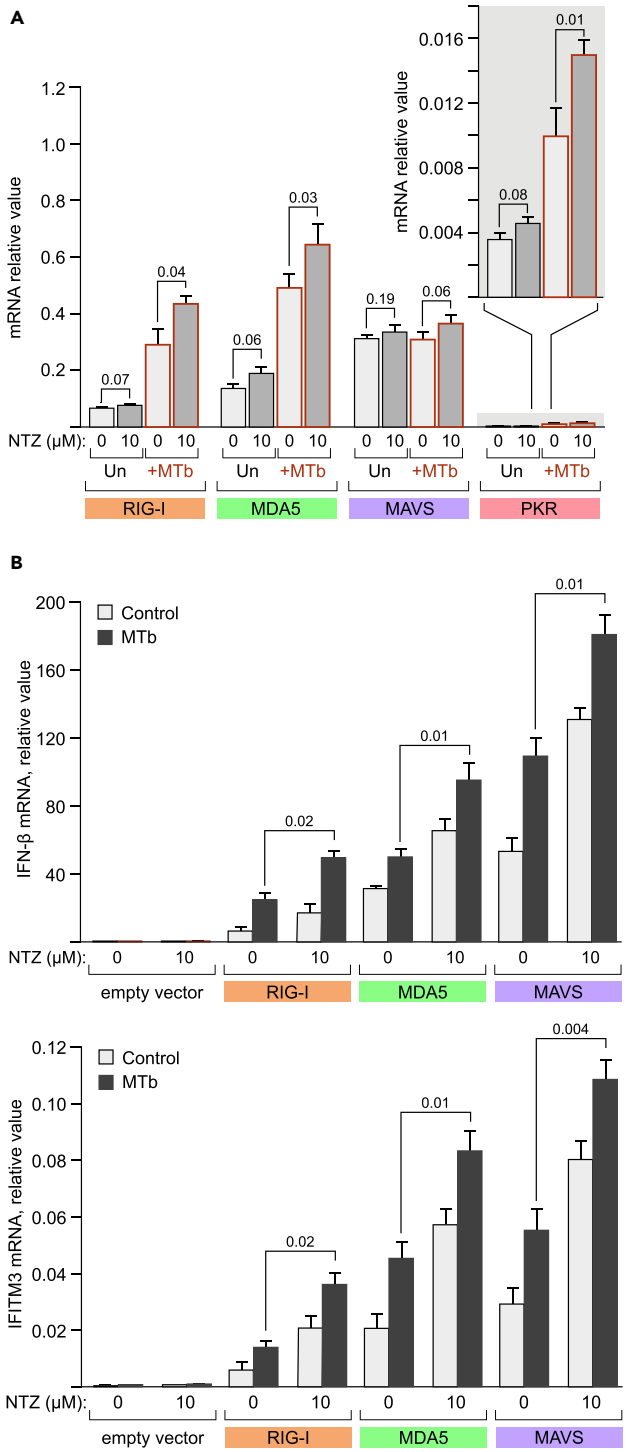

Figure 3. NTZ Enhances MTb-induced RLR and PKR Gene Expression and MTb-Activated RLR Activity

(A) mRNA levels of RIG-I, MDA5, MAVS, and PKR from THP-1 cells exposed to vehicle or 10 μM NTZ for 4 h and then infected with MTb (1:10 cell:bacilli) for 24 h, as indicated. Data were analyzed using the unpaired Student's t-test and are presented as mean ± SEM of three independent experiments.

(B) mRNA levels of IFN-β (top panel) or IFITM3 (bottom panel) from 293T cells transfected with empty vector or expression vectors for RIG-I, MDA5, or MAVS and treated with vehicle or with 10 μM NTZ for 4 h followed by 24 h of MTb infection as indicated. Data were analyzed using the unpaired Student's t-test and are presented as mean ± SEM of three independent experiments. Please see Figure S5 for examination of NTZ's effect on PKR phosphorylation.

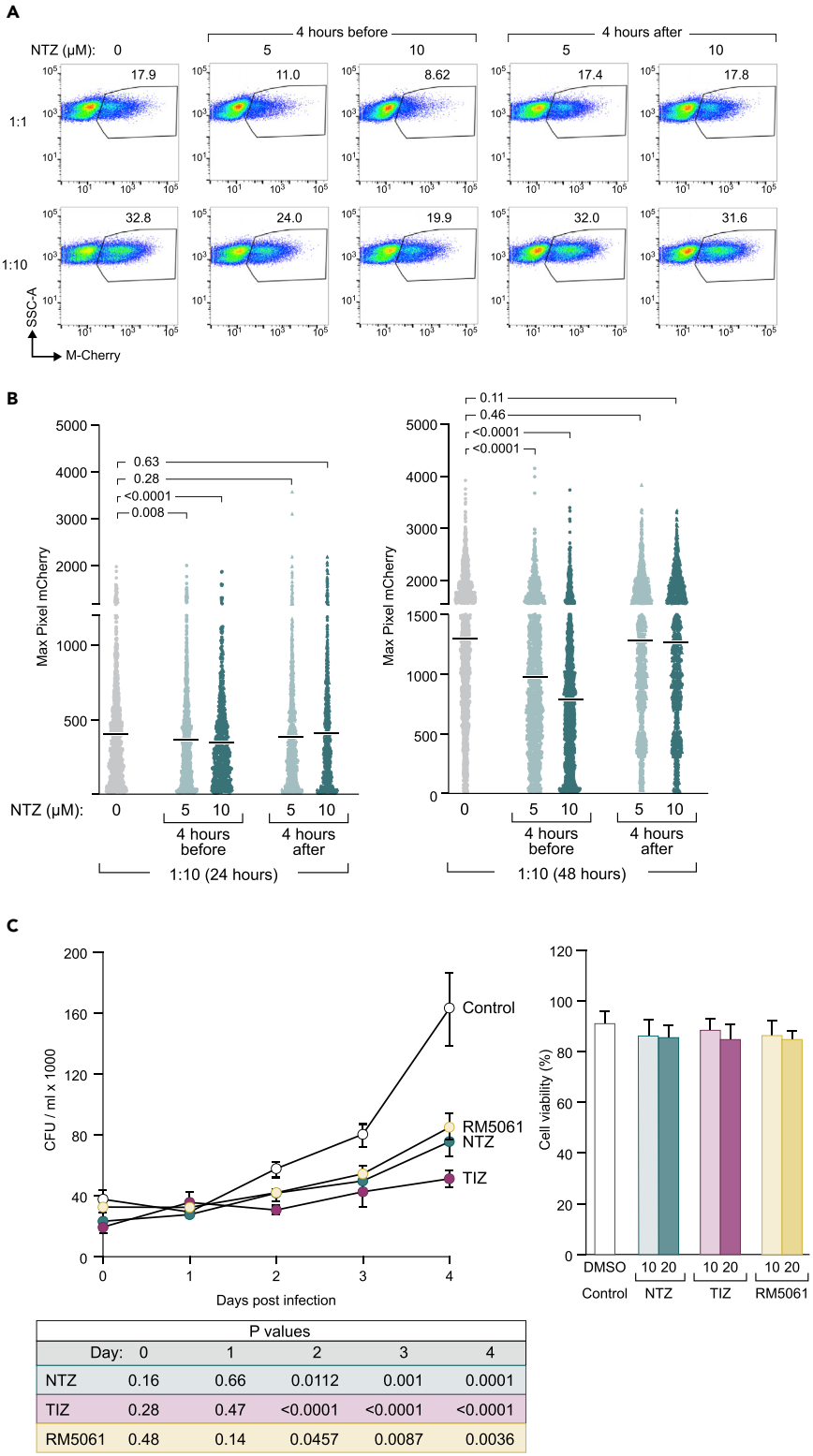

P values					
Day:	0	1	2	3	4
NTZ	0.16	0.66	0.0112	0.001	0.0001
TIZ	0.28	0.47	<0.0001	<0.0001	<0.0001
RM5061	0.48	0.14	0.0457	0.0087	0.0036

Figure 4. NTZ and NTZ derivatives Inhibit MTb Infection in Human Monocytic Cells and PBMC

(A) THP-1 cells were treated with 5 or 10 μM of NTZ 4 h before or 4 h after infection with MTb strain H37Rv-mCherry (1:1 cell:bacilli, top row; or 1:10 cell:bacilli, bottom row) for 20 h and analyzed by flow cytometry. Gated area and numerical values show the percentage of the cells infected with bacilli. Dot plots are representative of three independent experiments.

Figure 4. *Continued*

(B) Quantitative IFC analysis of THP-1 cells treated with 5 or 10 μM of NTZ 4 h before or 4 h after infection with MTb strain H37Rv-mCherry (1:10 cell:bacilli) for 24 or 48 h as indicated. Dot plot graphs show the pixel intensity of intracellular mCherry in the infected cells after ImageStream acquisition. Data were analyzed using the Mann-Whitney Test and are representative of three independent experiments, acquiring ~5,000 cells per sample each time.

(C) NTZ, TIZ, and RM5061 inhibit MTb in human PBMC. Left panel: CFU assay of normal PBMC at 0, 1, 2, 3, and 4 days after treatment with 10 μM of NTZ, TIZ, RM5061, or treated with vehicle as a control for 4 h followed by infection with H37Rv (1:10 cell: bacilli). Data were analyzed using the unpaired Student's t-test and are presented as mean ± SEM of four independent experiments in triplicate. Table shows complete statistics. Right panel: cell viability in response to increasing concentrations of NTZ and TIZ. Normal donor PBMC were treated with 10 or 20 μM of NTZ, TIZ, or RM5061, or treated with vehicle as a control for 24 h. Cells were harvested, stained with Annexin V-FITC, and subjected to flow cytometry analysis. Data were analyzed using the unpaired Student's t-test and are presented as mean ± SEM of four independent experiments.

primary human donor peripheral blood mononuclear cells (PBMC) from four individuals. For these experiments, we employed NTZ, its active circulating metabolite, tizoxanide (TIZ) (Rossignol, 2014), and a recently developed water-soluble prodrug derivative of TIZ, RM5061 (also known as aminoxanide or L-tert-leucyl thiazolide), which has a seven-fold higher blood concentration relative to NTZ in rats, with absolute bioavailability increasing from 3% to 20% (Stachulski et al., 2017) and which is in pre-clinical development for phase I human trials (Diawara et al., 2019). Pretreatment of donor PBMC with 10 μM NTZ, TIZ, or RM5061 for 4 h prior to MTb infection resulted in a highly significant reduction of MTb growth in the thiazolide drug-treated cultures after two (NTZ: $p = 0.0112$; TIZ: $p < 0.0001$; RM5061: $p = 0.0457$), three (NTZ: $p = 0.001$; TIZ: $p < 0.0001$; RM5061: $p = 0.0087$), and four (NTZ: $p = 0.0001$; TIZ: $p < 0.0001$; RM5061: $p = 0.0036$) days of MTb growth (Figure 4C, left).

In addition, there was no evidence of drug cytotoxicity based on the percentage of viable PBMCs detected by Annexin V-FITC staining following treatment with 10 or 20 μM NTZ, TIZ, or RM5061 relative to control cells for 24 h (Figure 4C, right). We note that 10 μM NTZ or TIZ is well below peak plasma levels of ~39 μM TIZ observed after an oral dose of 500 mg of NTZ (Stockis et al., 1996), which is a typical twice-a-day oral dosage of the drug (Stockis et al., 2002). Thus, taken together, these results demonstrate that NTZ, TIZ, or the new NTZ derivative RM5061 inhibits intracellular MTb growth in human cells measured using three distinct quantitative *in vitro* analyses, including by CFU in primary human PBMC.

DISCUSSION

Here we have shown that that RIG-I, MDA5, MAVS, and PKR each play a significant functional role in the cell-intrinsic control of intracellular MTb growth in human cells. Furthermore, we have shown that the broad expression and activity of the major RLR signaling proteins RIG-I, MDA5, and MAVS and the RLR-independent signaling protein PKR are increased by MTb infection of human cells. We have also demonstrated that the FDA-approved oral drug NTZ, which amplifies RLR, PKR, and interferon activities (Jasenosky et al., 2019), significantly inhibits MTb growth in human cells.

Two principal components of host cytoplasmic RNA surveillance, the RLR and PKR pathways, were initially characterized as part of the innate immune response to cytoplasmic viral RNA (Andrejeva et al., 2004; Bou-Nader et al., 2019; Kawai et al., 2005; Metz and Esteban, 1972; Meylan et al., 2005; Munir and Berg, 2013; Seth et al., 2005; Xu et al., 2005; Yoneyama et al., 2004, 2005). However, bacterial RNA can also interact with PKR (Bleiblo et al., 2012, 2013; Hull and Bevilacqua, 2015) and RLRs (Abdullah et al., 2012; Cheng and Schorey, 2018; Monroe et al., 2009; Rad et al., 2009). Independent findings using a murine system demonstrated a role for RIG-I and MAVS in MTb-induced IFN-β expression in macrophages (Cheng and Schorey, 2018). Furthermore, this group showed that MTb RNA-containing extracellular vesicles (EVs) isolated from MTb-infected cells promoted IFN-β expression and mycobacterial killing in recipient macrophages in an RIG-I- and MAVS-dependent fashion (Cheng and Schorey, 2019). These studies did not, however, examine the role of these sensors in inhibition of intracellular MTb growth within the initially infected host cell, nor did they reveal a role for MDA5 or PKR in these processes, nor the role of MTb in the induction of their transcription or activation.

By contrast, our data here show that two major proximal sensors in the RLR/MAVS cytosolic RNA surveillance pathway, RIG-I and MDA5, and the RLR-independent PKR pathway are induced by MTb infection and play non-redundant roles in the cell-intrinsic response to inhibit MTb growth. We note that RIG-I

and MDA5 recognize their RNA ligands via distinct mechanisms prior to their interaction with MAVS (Gebhardt et al., 2017; Reikine et al., 2014; Tatematsu et al., 2018). RIG-I binds to the ends of short dsRNAs, exhibiting a preference for blunt ends and 5′ triphosphates (Hornung et al., 2006; Kato et al., 2006; Pichlmair et al., 2006), and then assembles into tetrameric structures (Peisley et al., 2013, 2014). By contrast, MDA5 binds to internal sequences, rather than the ends, of long dsRNAs, assembling cooperatively into filaments along the RNA (Berke and Modis, 2012; Peisley et al., 2011, 2013; Wu et al., 2013). The multimerization of RIG-I or MDA5, in turn, promotes the aggregation of MAVS at the mitochondrial membrane, leading to downstream signaling (Berke and Modis, 2012; Hou et al., 2011; Jiang et al., 2012; Peisley et al., 2011, 2014; Shi et al., 2015; Wu et al., 2014). Thus, our data indicate that MTb RNAs expressed during active MTb infection can trigger both the RIG-I and MDA5 arms of the RLR pathway.

The mechanism and function of PKR is distinct from the RLR/MAVS pathway (Bou-Nader et al., 2019; Hull and Bevilacqua, 2016; Munir and Berg, 2013). Instead of triggering activation of MAVS, leading to activation of the transcription factor IRF3 (Gebhardt et al., 2017; Reikine et al., 2014; Tatematsu et al., 2018), PKR is involved in shutdown of protein synthesis via phosphorylation of eIF2α and can directly or indirectly activate kinase pathways, including MAP kinases and those leading to NF-κB activation resulting in innate immune gene expression (Bou-Nader et al., 2019; Dalet et al., 2015; Gal-Ben-Ari et al., 2018; Gebhardt et al., 2017; Hull and Bevilacqua, 2016; Munir and Berg, 2013). Furthermore, PKR can be activated by a number of stimuli apart from RNA, such as TLR engagement, oxidative stress, growth factors, and cytokines (Bou-Nader et al., 2019; Dalet et al., 2015; Gal-Ben-Ari et al., 2018; Munir and Berg, 2013). Early studies showed that the PKR inhibitor 2-aminopurine inhibited lipopolysaccharide-driven TNF gene expression (Goldfeld and Maniatis, 1989). *Mycobacterium bovis* bacillus Calmette-Guérin (BCG) was later found to induce transcription of TNF, interleukin 6 (IL-6), and IL-10, as well as promote phosphorylation of PKR in a 2-aminopurine-sensitive fashion (Cheung et al., 2005). As an RNA sensor, PKR responds to multiple synthetic and viral DNAs, undergoing dimerization induced by dsRNA interaction as well as other stimuli (Bou-Nader et al., 2019; Hull and Bevilacqua, 2016).

Although PKR's role in IFN-β gene expression has been characterized by a number of studies (Dalet et al., 2015; Gal-Ben-Ari et al., 2018; Munir and Berg, 2013), PKR's role in TB has not been clarified. Although a previous study reported that $PKR^{-/-}$ mice had a reduced MTb burden (Wu et al., 2012); the same group later attributed that finding to an error in mouse strain background and not to PKR directly (Mundhra et al., 2018). Here, we have shown that MTb infection causes an increase in PKR mRNA and protein levels and in phosphorylation of its substrate eIF2α in human cells. Furthermore, we have shown that PKR deficiency results in significantly enhanced intracellular MTb growth by both IFC and CFU analyses. Taken together, our studies thus demonstrate that proteins of both the RLR/MAVS and PKR cytoplasmic RNA sensor pathways are critical components of host restriction of intracellular MTb growth in human cells.

Here, we have also shown that NTZ broadly enhances MTb-driven RLR/MAVS activities, resulting in increased IFITM3 and IFN-β gene expression, and that it increases gene expression of RIG-I, MDA5, and PKR, extending the immunomodulatory effect of NTZ to antimycobacterial host gene activity. The details of how MTb infection regulates expression of the host RNA sensing pathway, the role of type I IFNs, and how NTZ amplifies these effects in TB pathogenesis remain to be explored further. We also observed that, similar to MTb infection, MTb lysate increased mRNA expression of the ISGs RIG-I, MDA5, PKR, and IFITM3. MTb glycolipoproteins, lipoproteins, and glycolipids present in the lysate are ligands for TLR4 and TLR2, which can in turn trigger activation of IRF3 and, more broadly, type I IFNs (Falvo et al., 2011; Perkins and Vogel, 2015); thus, the TLR and IRF/IFN pathways may play a complementary role in this context. Indeed, we note that there is evidence that IRF3 can regulate the gene promoters of both RIG-I and MDA5 (Hayakari et al., 2016; Yount et al., 2007) and that interferon-stimulated gene factor 3 (ISGF-3) can regulate the PKR gene promoter (Ward and Samuel, 2003). Furthermore, given that NTZ can promote IRF3-driven IFN-β mRNA expression in addition to its ability to broadly amplify RLR activity (Jasenosky et al., 2019), it is intriguing to speculate that MTb and NTZ directly enhance gene expression of sensor molecules via their effects on upstream transcriptional activators.

Finally, our demonstration of the key role of cytoplasmic RNA sensor proteins in the cell-intrinsic control of MTb growth and the ability of NTZ to amplify their effects suggest them as attractive targets for chemical regulation to inhibit MTb. Current antimycobacterial treatment regimens are long and complex, complicated by evolving drug resistance and a large burden of disease caused by multi-drug resistant TB (Bloom et al., 2017). NTZ has a long track record of safety, including in HIV co-infected individuals (Abubakar et al.,

2007). It is of low cost and available as an oral agent, including as a pediatric syrup formulation (Rossignol, 2014), making it an easily scalable treatment for adults and children. Our demonstration here showing highly significant NTZ inhibition of intracellular MTb growth in THP-1 cells and in donor PMBCs thus also provides support for the repurposing of NTZ, or newer NTZ derivatives, as a host-directed TB therapy to complement canonical TB treatment regimens.

Limitations of the Study

We have not yet established the role of type I IFNs in MTb induction of RNA sensor transcription or the role of type I IFNs in NTZ's amplification of MTb-driven RNA sensor activities. These studies, as well as the investigation and identification of NTZ's upstream target(s) are outside the scope of this article and will be the subject of future research.

METHODS

All methods can be found in the accompanying Transparent Methods supplemental file.

SUPPLEMENTAL INFORMATION

Supplemental Information can be found online at https://doi.org/10.1016/j.isci.2019.11.001.

ACKNOWLEDGMENTS

This work was supported by grants from the NIH (AI125075), the Annenberg Foundation, the Ragon Institute, and by lab gifts from Romark Inc., and from John Moores and Jeanne Sullivan to A.E.G., and, by a grant from the Campbell Foundation to S.R. The funders had no role in the conceptualization, design, data collection, analysis, decision to publish, or preparation of the manuscript. We thank Sun Hur for helpful discussions and advice. We are grateful to Jean-Francois Rossignol for his encouragement, to Stefan Kaufmann for critical reading of the manuscript, and to Renate Hellmiss for the artwork.

AUTHOR CONTRIBUTIONS

Methodology: S.R., V.H., L.D.J., and A.N.; Investigation: S.R., V.H., A.N., and S.S.; Validation: S.R., V.H., L.D.J., A.N., and A.E.G.; Writing: Original Draft, A.E.G. and J.V.F.; Review & Editing: A.E.G., J.V.F., and S.R.; Visualization: V.H., S.R., and A.E.G; Resources: T.S.E. and V.H.; Funding Acquisition: S.R., A.E.G., and G.H.C.; Conceptualization and Supervision: A.E.G.

DECLARATION OF INTERESTS

L.D.J., S.R., V.H., and A.E.G. are co-inventors on the patent "Treatment of Infectious Diseases," US15/546390 Jan 26 2015. The authors claim no other competing interests.

Received: August 26, 2019
Revised: October 2, 2019
Accepted: October 30, 2019
Published: December 20, 2019

REFERENCES

Abdullah, Z., Schlee, M., Roth, S., Mraheil, M.A., Barchet, W., Bottcher, J., Hain, T., Geiger, S., Hayakawa, Y., Fritz, J.H., et al. (2012). RIG-I detects infection with live *Listeria* by sensing secreted bacterial nucleic acids. EMBO J. *31*, 4153–4164.

Ablasser, A., Goldeck, M., Cavlar, T., Deimling, T., Witte, G., Rohl, I., Hopfner, K.P., Ludwig, J., and Hornung, V. (2013). cGAS produces a 2′-5′-linked cyclic dinucleotide second messenger that activates STING. Nature *498*, 380–384.

Abubakar, I., Aliyu, S.H., Arumugam, C., Usman, N.K., and Hunter, P.R. (2007). Treatment of cryptosporidiosis in immunocompromised individuals: systematic review and meta-analysis. Br. J. Clin. Pharmacol. *63*, 387–393.

Ahmad, S., Mu, X., Yang, F., Greenwald, E., Park, J.W., Jacob, E., Zhang, C.Z., and Hur, S. (2018). Breaching self-tolerance to alu duplex RNA underlies MDA5-mediated inflammation. Cell *172*, 797–810.e13.

Anderson, V.R., and Curran, M.P. (2007). Nitazoxanide: a review of its use in the treatment of gastrointestinal infections. Drugs *67*, 1947–1967.

Andrejeva, J., Childs, K.S., Young, D.F., Carlos, T.S., Stock, N., Goodbourn, S., and Randall, R.E. (2004). The V proteins of paramyxoviruses bind the IFN-inducible RNA helicase, mda-5, and inhibit its activation of the IFN-β promoter. Proc. Natl. Acad. Sci. U S A *101*, 17264–17269.

Andreu, N., Phelan, J., de Sessions, P.F., Cliff, J.M., Clark, T.G., and Hibberd, M.L. (2017). Primary macrophages and J774 cells respond differently to infection with *Mycobacterium tuberculosis*. Sci. Rep. *7*, 42225.

Ashiru, O., Howe, J.D., and Butters, T.D. (2014). Nitazoxanide, an antiviral thiazolide, depletes ATP-sensitive intracellular Ca(2+) stores. Virology *462-463*, 135–148.

Barthel, R., Tsytsykova, A.V., Barczak, A.K., Tsai, E.Y., Dascher, C.C., Brenner, M.B., and Goldfeld, A.E. (2003). Regulation of tumor necrosis factor alpha gene expression by mycobacteria involves the assembly of a unique enhanceosome dependent on the coactivator proteins CBP/p300. Mol. Cell Biol. *23*, 526–533.

Basiji, D.A., Ortyn, W.E., Liang, L., Venkatachalam, V., and Morrissey, P. (2007). Cellular image analysis and imaging by flow cytometry. Clin. Lab. Med. *27*, 653–670.

Berke, I.C., and Modis, Y. (2012). MDA5 cooperatively forms dimers and ATP-sensitive filaments upon binding double-stranded RNA. EMBO J. *31*, 1714–1726.

Bleiblo, F., Michael, P., Brabant, D., Ramana, C.V., Tai, T., Saleh, M., Parrillo, J.E., Kumar, A., and Kumar, A. (2012). Bacterial RNA induces myocyte cellular dysfunction through the activation of PKR. J. Thorac. Dis. *4*, 114–125.

Bleiblo, F., Michael, P., Brabant, D., Ramana, C.V., Tai, T., Saleh, M., Parrillo, J.E., Kumar, A., and Kumar, A. (2013). JAK kinases are required for the bacterial RNA and poly I: C induced tyrosine phosphorylation of PKR. Int. J. Clin. Exp. Med. *6*, 16–25.

Bloom, B.R., Atun, R., Cohen, T., Dye, C., Fraser, H., Gomez, G.B., Knight, G., Murray, M., Nardell, E., Rubin, E., et al. (2017). Tuberculosis. In Major Infectious Diseases, Rd, K.K. Holmes, S. Bertozzi, B.R. Bloom, and P. Jha, eds. (The International Bank for Reconstruction and Development), pp. 233–313.

Bou-Nader, C., Gordon, J.M., Henderson, F.E., and Zhang, J. (2019). The search for a PKR code-differential regulation of protein kinase R activity by diverse RNA and protein regulators. RNA *25*, 539–556.

Carroll, K., Elroy-Stein, O., Moss, B., and Jagus, R. (1993). Recombinant vaccinia virus K3L gene product prevents activation of double-stranded RNA-dependent, initiation factor 2α-specific protein kinase. J. Biol. Chem. *268*, 12837–12842.

Cavanaugh, J.S., Jou, R., Wu, M.H., Dalton, T., Kurbatova, E., Ershova, J., Cegielski, J.P., and Global, P.I. (2017). Susceptibilities of MDR *Mycobacterium tuberculosis* isolates to unconventional drugs compared with their reported pharmacokinetic/pharmacodynamic parameters. J. Antimicrob. Chemother. *72*, 1678–1687.

Cheng, Y., and Schorey, J.S. (2018). *Mycobacterium tuberculosis*-induced IFN-β production requires cytosolic DNA and RNA sensing pathways. J. Exp. Med. *215*, 2919–2935.

Cheng, Y., and Schorey, J.S. (2019). Extracellular vesicles deliver *Mycobacterium* RNA to promote host immunity and bacterial killing. EMBO Rep. *20*, e46613.

Cheung, B.K., Lee, D.C., Li, J.C., Lau, Y.L., and Lau, A.S. (2005). A role for double-stranded RNA-activated protein kinase PKR in *Mycobacterium*-induced cytokine expression. J. Immunol. *175*, 7218–7225.

Collins, A.C., Cai, H., Li, T., Franco, L.H., Li, X.D., Nair, V.R., Scharn, C.R., Stamm, C.E., Levine, B., Chen, Z.J., et al. (2015). Cyclic GMP-AMP synthase is an innate immune DNA sensor for *Mycobacterium tuberculosis*. Cell Host Microbe *17*, 820–828.

Cui, J., Chen, Y., Wang, H.Y., and Wang, R.F. (2014). Mechanisms and pathways of innate immune activation and regulation in health and cancer. Hum. Vaccin. Immunother. *10*, 3270–3285.

Daher Ede, F., da Silva, G.B., Jr., and Barros, E.J. (2013). Renal tuberculosis in the modern era. Am. J. Trop. Med. Hyg. *88*, 54–64.

Dalet, A., Gatti, E., and Pierre, P. (2015). Integration of PKR-dependent translation inhibition with innate immunity is required for a coordinated anti-viral response. FEBS Lett. *589*, 1539–1545.

de Carvalho, L.P., Darby, C.M., Rhee, K.Y., and Nathan, C. (2011). Nitazoxanide disrupts membrane potential and intrabacterial pH homeostasis of *Mycobacterium tuberculosis*. ACS Med. Chem. Lett. *2*, 849–854.

de Carvalho, L.P., Lin, G., Jiang, X., and Nathan, C. (2009). Nitazoxanide kills replicating and nonreplicating *Mycobacterium tuberculosis* and evades resistance. J. Med. Chem. *52*, 5789–5792.

Dey, B., Dey, R.J., Cheung, L.S., Pokkali, S., Guo, H., Lee, J.H., and Bishai, W.R. (2015). A bacterial cyclic dinucleotide activates the cytosolic surveillance pathway and mediates innate resistance to tuberculosis. Nat. Med. *21*, 401–406.

Diawara, E.H., Razakandrainibe, H.T.R., Rossignol, J.-F., Stachulski, A., Le Goff, L., François, A., Favennec, L.., and Gargala, G.C. (2019). Parental aminoxanide as a novel treatment against cryptosporidiosis. Paper presented at: 29th European Congress of Clinical Microbiology and Infectious Diseases (Amsterdam, Netherlands).

Doan, M., Vorobjev, I., Rees, P., Filby, A., Wolkenhauer, O., Goldfeld, A.E., Lieberman, J., Barteneva, N., Carpenter, A.E., and Hennig, H. (2018). Diagnostic potential of imaging flow cytometry. Trends Biotechnol. *36*, 649–652.

Elazar, M., Liu, M., McKenna, S.A., Liu, P., Gehrig, E.A., Puglisi, J.D., Rossignol, J.-F., and Glenn, J.S. (2009). The anti-hepatitis C agent nitazoxanide induces phosphorylation of eukaryotic initiation factor 2α via protein kinase activated by double-stranded RNA activation. Gastroenterology *137*, 1827–1835.

Falvo, J.V., Ranjbar, S., Jasenosky, L.D., and Goldfeld, A.E. (2011). Arc of a vicious circle: pathways activated by *Mycobacterium tuberculosis* that target the HIV-1 LTR. Am. J. Respir. Cell Mol. Biol. *45*, 1116–1124.

Gaidt, M.M., Ebert, T.S., Chauhan, D., Ramshorn, K., Pinci, F., Zuber, S., O'Duill, F., Schmid-Burgk, J.L., Hoss, F., Buhmann, R., et al. (2017). The DNA inflammasome in human myeloid cells is initiated by a STING-cell death program upstream of NLRP3. Cell *171*, 1110–1124.e8.

Gal-Ben-Ari, S., Barrera, I., Ehrlich, M., and Rosenblum, K. (2018). PKR: a kinase to remember. Front. Mol. Neurosci. *11*, 480.

Galabru, J., and Hovanessian, A. (1987). Autophosphorylation of the protein kinase dependent on double-stranded RNA. J. Biol. Chem. *262*, 15538–15544.

Gebhardt, A., Laudenbach, B.T., and Pichlmair, A. (2017). Discrimination of self and non-self ribonucleic acids. J. Interferon. Cytokine Res. *37*, 184–197.

Harausz, E.P., Chervenak, K.A., Good, C.E., Jacobs, M.R., Wallis, R.S., Sanchez-Felix, M., and Boom, W.H.; TB Research Unit at Case Western Reserve University (2016). Activity of nitazoxanide and tizoxanide against *Mycobacterium tuberculosis* in vitro and in whole blood culture. Tuberculosis (Edinb.) *98*, 92–96.

Haridas, V., Ranjbar, S., Vorobjev, I.A., Goldfeld, A.E., and Barteneva, N.S. (2017). Imaging flow cytometry analysis of intracellular pathogens. Methods *112*, 91–104.

Hayakari, R., Matsumiya, T., Xing, F., Yoshida, H., Hayakari, M., and Imaizumi, T. (2016). Critical role of IRF-3 in the direct regulation of dsRNA-induced retinoic acid-inducible gene-I (RIG-I) expression. PLoS One *11*, e0163520.

Hickson, S.E., Margineantu, D., Hockenbery, D.M., Simon, J.A., and Geballe, A.P. (2018). Inhibition of vaccinia virus replication by nitazoxanide. Virology *518*, 398–405.

Hornung, V., Ellegast, J., Kim, S., Brzozka, K., Jung, A., Kato, H., Poeck, H., Akira, S., Conzelmann, K.K., Schlee, M., et al. (2006). 5′-Triphosphate RNA is the ligand for RIG-I. Science *314*, 994–997.

Hou, F., Sun, L., Zheng, H., Skaug, B., Jiang, Q.X., and Chen, Z.J. (2011). MAVS forms functional prion-like aggregates to activate and propagate antiviral innate immune response. Cell *146*, 448–461.

Hull, C.M., and Bevilacqua, P.C. (2015). Mechanistic analysis of activation of the innate immune sensor PKR by bacterial RNA. J. Mol. Biol. *427*, 3501–3515.

Hull, C.M., and Bevilacqua, P.C. (2016). Discriminating self and non-self by RNA: roles for RNA structure, misfolding, and modification in regulating the innate immune sensor PKR. Acc. Chem. Res. *49*, 1242–1249.

Hurtado, R.M., Meressa, D., and Goldfeld, A.E. (2018). Treatment of drug-resistant tuberculosis among people living with HIV. Curr. Opin. HIV AIDS *13*, 478–485.

Janulionis, E., Sofer, C., Song, H.Y., and Wallis, R.S. (2004). Lack of activity of orally administered clofazimine against intracellular *Mycobacterium tuberculosis* in whole-blood culture. Antimicrob. Agents Chemother. *48*, 3133–3135.

Jasenosky, L.D., Cadena, C., Mire, C.E., Borisevich, V., Haridas, V., Ranjbar, S., Nambu, A., Bavari, S., Soloveva, V., Sadukhan, S., et al. (2019). The FDA-approved oral drug nitazoxanide amplifies host antiviral responses and inhibits Ebola virus. iScience *19*, 1279–1290.

Jiang, X., Kinch, L.N., Brautigam, C.A., Chen, X., Du, F., Grishin, N.V., and Chen, Z.J. (2012). Ubiquitin-induced oligomerization of the RNA sensors RIG-I and MDA5 activates antiviral innate immune response. Immunity *36*, 959–973.

Kato, H., Takeuchi, O., Mikamo-Satoh, E., Hirai, R., Kawai, T., Matsushita, K., Hiiragi, A., Dermody, T.S., Fujita, T., and Akira, S. (2008). Length-dependent recognition of double-stranded ribonucleic acids by retinoic acid-inducible gene-I and melanoma differentiation-associated gene 5. J. Exp. Med. *205*, 1601–1610.

Kato, H., Takeuchi, O., Sato, S., Yoneyama, M., Yamamoto, M., Matsui, K., Uematsu, S., Jung, A., Kawai, T., Ishii, K.J., et al. (2006). Differential roles of MDA5 and RIG-I helicases in the recognition of RNA viruses. Nature *441*, 101–105.

Katze, M.G., Wambach, M., Wong, M.L., Garfinkel, M., Meurs, E., Chong, K., Williams, B.R., Hovanessian, A.G., and Barber, G.N. (1991). Functional expression and RNA binding analysis of the interferon-induced, double-stranded RNA-activated, 68,000-Mr protein kinase in a cell-free system. Mol. Cell Biol. *11*, 5497–5505.

Kaufmann, S.H., and Dorhoi, A. (2013). Inflammation in tuberculosis: interactions, imbalances and interventions. Curr. Opin. Immunol. *25*, 441–449.

Kawai, T., Takahashi, K., Sato, S., Coban, C., Kumar, H., Kato, H., Ishii, K.J., Takeuchi, O., and Akira, S. (2005). IPS-1, an adaptor triggering RIG-I- and Mda5-mediated type I interferon induction. Nat. Immunol. *6*, 981–988.

Kawasaki, T., and Kawai, T. (2019). Discrimination between self and non-self-nucleic acids by the innate immune system. Int. Rev. Cell Mol. Biol. *344*, 1–30.

Lam, K.K.Y., Zheng, X., Forestieri, R., Balgi, A.D., Nodwell, M., Vollett, S., Anderson, H.J., Andersen, R.J., Av-Gay, Y., and Roberge, M. (2012). Nitazoxanide stimulates autophagy and inhibits mTORC1 signaling and intracellular proliferation of *Mycobacterium tuberculosis*. PLoS Pathog. *8*, e1002691.

Mankan, A.K., Schmidt, T., Chauhan, D., Goldeck, M., Höning, K., Gaidt, M., Kubarenko, A.V., Andreeva, L., Hopfner, K.P., and Hornung, V. (2014). Cytosolic RNA: DNA hybrids activate the cGAS-STING axis. EMBO J. *33*, 2937–2946.

Manzanillo, P.S., Shiloh, M.U., Portnoy, D.A., and Cox, J.S. (2012). *Mycobacterium tuberculosis* activates the DNA-dependent cytosolic surveillance pathway within macrophages. Cell Host Microbe *11*, 469–480.

Metz, D.H., and Esteban, M. (1972). Interferon inhibits viral protein synthesis in L cells infected with vaccinia virus. Nature *238*, 385–388.

Meurs, E., Chong, K., Galabru, J., Thomas, N.S., Kerr, I.M., Williams, B.R., and Hovanessian, A.G. (1990). Molecular cloning and characterization of the human double-stranded RNA-activated protein kinase induced by interferon. Cell *62*, 379–390.

Meylan, E., Curran, J., Hofmann, K., Moradpour, D., Binder, M., Bartenschlager, R., and Tschopp, J. (2005). Cardif is an adaptor protein in the RIG-I antiviral pathway and is targeted by hepatitis C virus. Nature *437*, 1167–1172.

Monroe, K.M., McWhirter, S.M., and Vance, R.E. (2009). Identification of host cytosolic sensors and bacterial factors regulating the type I interferon response to Legionella pneumophila. PLoS Pathog. *5*, e1000665.

Moreira-Teixeira, L., Mayer-Barber, K., Sher, A., and O'Garra, A. (2018). Type I interferons in tuberculosis: foe and occasionally friend. J. Exp. Med. *215*, 1273–1285.

Mundhra, S., Bryk, R., Hawryluk, N., Zhang, T., Jiang, X., and Nathan, C.F. (2018). Evidence for dispensability of protein kinase R in host control of tuberculosis. Eur. J. Immunol. *48*, 612–620.

Munir, M., and Berg, M. (2013). The multiple faces of proteinkinase R in antiviral defense. Virulence *4*, 85–89.

Odingo, J., Bailey, M.A., Files, M., Early, J.V., Alling, T., Dennison, D., Bowman, J., Dalai, S., Kumar, N., Cramer, J., et al. (2017). Vitro evaluation of novel nitazoxanide derivatives against *Mycobacterium tuberculosis*. ACS Omega *2*, 5873–5890.

Paijo, J., Doring, M., Spanier, J., Grabski, E., Nooruzzaman, M., Schmidt, T., Witte, G., Messerle, M., Hornung, V., Kaever, V., et al. (2016). cGAS senses human cytomegalovirus and induces type I interferon responses in human monocyte-derived cells. PLoS Pathog. *12*, e1005546.

Pandey, S., Kawai, T., and Akira, S. (2014). Microbial sensing by Toll-like receptors and intracellular nucleic acid sensors. Cold Spring Harb Perspect. Biol. *7*, a016246.

Peisley, A., Lin, C., Wu, B., Orme-Johnson, M., Liu, M., Walz, T., and Hur, S. (2011). Cooperative assembly and dynamic disassembly of MDA5 filaments for viral dsRNA recognition. Proc. Natl. Acad. Sci. U S A *108*, 21010–21015.

Peisley, A., Wu, B., Xu, H., Chen, Z.J., and Hur, S. (2014). Structural basis for ubiquitin-mediated antiviral signal activation by RIG-I. Nature *509*, 110–114.

Peisley, A., Wu, B., Yao, H., Walz, T., and Hur, S. (2013). RIG-I forms signaling-competent filaments in an ATP-dependent, ubiquitin-independent manner. Mol. Cell *51*, 573–583.

Perkins, D.J., and Vogel, S.N. (2015). Space and time: new considerations about the relationship between Toll-like receptors (TLRs) and type I interferons (IFNs). Cytokine *74*, 171–174.

Piccaro, G., Giannoni, F., Filippini, P., Mustazzolu, A., and Fattorini, L. (2013). Activities of drug combinations against *Mycobacterium tuberculosis* grown in aerobic and hypoxic acidic conditions. Antimicrob. Agents Chemother. *57*, 1428–1433.

Pichlmair, A., Schulz, O., Tan, C.P., Naslund, T.I., Liljestrom, P., Weber, F., and Reis e Sousa, C. (2006). RIG-I-mediated antiviral responses to single-stranded RNA bearing 5'-phosphates. Science *314*, 997–1001.

Rad, R., Ballhorn, W., Voland, P., Eisenacher, K., Mages, J., Rad, L., Ferstl, R., Lang, R., Wagner, H., Schmid, R.M., et al. (2009). Extracellular and intracellular pattern recognition receptors cooperate in the recognition of *Helicobacter pylori*. Gastroenterology *136*, 2247–2257.

Ranjbar, S., Haridas, V., Jasenosky, L.D., Falvo, J.V., and Goldfeld, A.E. (2015). A role for IFITM proteins in restriction of *Mycobacterium tuberculosis* infection. Cell Rep. *13*, 874–883.

Ranjbar, S., Jasenosky, L.D., Chow, N., and Goldfeld, A.E. (2012). Regulation of *Mycobacterium tuberculosis*-dependent HIV-1 transcription reveals a new role for NFAT5 in the toll-like receptor pathway. PLoS Pathog. *8*, e1002620.

Reikine, S., Nguyen, J.B., and Modis, Y. (2014). Pattern recognition and signaling mechanisms of RIG-I and MDA5. Front. Immunol. *5*, 342.

Rossignol, J.-F. (2014). Nitazoxanide: a first-in-class broad-spectrum antiviral agent. Antivir. Res. *110*, 94–103.

Sangana, R., Gu, H., Chun, D.Y., and Einolf, H.J. (2018). Evaluation of clinical drug interaction potential of clofazimine using static and dynamic modeling approaches. Drug Metab. Dispos. *46*, 26–32.

Schmid-Burgk, J.L., Schmidt, T., Gaidt, M.M., Pelka, K., Latz, E., Ebert, T.S., and Hornung, V. (2014). OutKnocker: a web tool for rapid and simple genotyping of designer nuclease edited cell lines. Genome Res. *24*, 1719–1723.

Seth, R.B., Sun, L., Ea, C.K., and Chen, Z.J. (2005). Identification and characterization of MAVS, a mitochondrial antiviral signaling protein that activates NF-kB and IRF 3. Cell *122*, 669–682.

Shi, Y., Yuan, B., Qi, N., Zhu, W., Su, J., Li, X., Qi, P., Zhang, D., and Hou, F. (2015). An autoinhibitory mechanism modulates MAVS activity in antiviral innate immune response. Nat. Commun. *6*, 7811.

Shigyo, K., Ocheretina, O., Merveille, Y.M., Johnson, W.D., Pape, J.W., Nathan, C.F., and Fitzgerald, D.W. (2013). Efficacy of nitazoxanide against clinical isolates of *Mycobacterium tuberculosis*. Antimicrob. Agents Chemother. *57*, 2834–2837.

Sillé, F.C., Martin, C., Jayaraman, P., Rothchild, A., Fortune, S., Besra, G.S., Behar, S.M., and Boes, M. (2011). Requirement for invariant chain in macrophages for *Mycobacterium tuberculosis* replication and CD1d antigen presentation. Infect. Immun. *79*, 3053–3063.

Stachulski, A.V., Swift, K., Cooper, M., Reynolds, S., Norton, D., Slonecker, S.D., and Rossignol, J.-F. (2017). Synthesis and pre-clinical studies of new amino-acid ester thiazolide prodrugs. Eur. J. Med. Chem. *126*, 154–159.

Stockis, A., De Bruyn, S., Gengler, C., and Rosillon, D. (2002). Nitazoxanide pharmacokinetics and tolerability in man during 7 days dosing with 0.5 g and 1 g b.i.d. Int. J. Clin. Pharmacol. Ther. *40*, 221–227.

Stockis, A., Deroubaix, X., Lins, R., Jeanbaptiste, B., Calderon, P., and Rossignol, J.-F. (1996). Pharmacokinetics of nitazoxanide after single oral dose administration in 6 healthy volunteers. Int. J. Clin. Pharmacol. Ther. *34*, 349–351.

Tatematsu, M., Funami, K., Seya, T., and Matsumoto, M. (2018). Extracellular RNA sensing by pattern recognition receptors. J. Innate Immun. *10*, 398–406.

Thomis, D.C., and Samuel, C.E. (1993). Mechanism of interferon action: evidence for intermolecular autophosphorylation and autoactivation of the interferon-induced, RNA-dependent protein kinase PKR. J. Virol. *67*, 7695–7700.

Wallis, R.S., Vinhas, S.A., Johnson, J.L., Ribeiro, F.C., Palaci, M., Peres, R.L., Sa, R.T., Dietze, R., Chiunda, A., Eisenach, K., et al. (2003). Whole blood bactericidal activity during treatment of pulmonary tuberculosis. J. Infect. Dis. *187*, 270–278.

Ward, S.V., and Samuel, C.E. (2003). The PKR kinase promoter binds both Sp1 and Sp3, but only Sp3 functions as part of the interferon-inducible complex with ISGF-3 proteins. Virology *313*, 553–566.

Wassermann, R., Gulen, M.F., Sala, C., Perin, S.G., Lou, Y., Rybniker, J., Schmid-Burgk, J.L., Schmidt, T., Hornung, V., Cole, S.T., et al. (2015). *Mycobacterium tuberculosis* differentially activates cGAS- and inflammasome-dependent intracellular immune responses through ESX-1. Cell Host Microbe *17*, 799–810.

Watson, R.O., Bell, S.L., MacDuff, D.A., Kimmey, J.M., Diner, E.J., Olivas, J., Vance, R.E., Stallings, C.L., Virgin, H.W., and Cox, J.S. (2015). The cytosolic sensor cGAS detects *Mycobacterium tuberculosis* DNA to induce type I interferons and activate autophagy. Cell Host Microbe *17*, 811–819.

Wu, B., and Hur, S. (2015). How RIG-I like receptors activate MAVS. Curr. Opin. Virol. *12*, 91–98.

Wu, B., Peisley, A., Richards, C., Yao, H., Zeng, X., Lin, C., Chu, F., Walz, T., and Hur, S. (2013). Structural basis for dsRNA recognition, filament formation, and antiviral signal activation by MDA5. Cell *152*, 276–289.

Wu, B., Peisley, A., Tetrault, D., Li, Z., Egelman, E.H., Magor, K.E., Walz, T., Penczek, P.A., and Hur, S. (2014). Molecular imprinting as a signal-activation mechanism of the viral RNA sensor RIG-I. Mol. Cell *55*, 511–523.

Wu, K., Koo, J., Jiang, X., Chen, R., Cohen, S.N., and Nathan, C. (2012). Improved control of tuberculosis and activation of macrophages in mice lacking protein kinase R. PLoS One *7*, e30512.

Xu, L.G., Wang, Y.Y., Han, K.J., Li, L.Y., Zhai, Z., and Shu, H.B. (2005). VISA is an adapter protein required for virus-triggered IFN-β signaling. Mol. Cell *19*, 727–740.

Yao, H., Dittmann, M., Peisley, A., Hoffmann, H.H., Gilmore, R.H., Schmidt, T., Schmidt-Burgk, J., Hornung, V., Rice, C.M., and Hur, S. (2015). ATP-dependent effector-like functions of RIG-I-like receptors. Mol. Cell *58*, 541–548.

Yoneyama, M., Kikuchi, M., Matsumoto, K., Imaizumi, T., Miyagishi, M., Taira, K., Foy, E., Loo, Y.M., Gale, M., Jr., Akira, S., et al. (2005). Shared and unique functions of the DExD/H-box helicases RIG-I, MDA5, and LGP2 in antiviral innate immunity. J. Immunol. *175*, 2851–2858.

Yoneyama, M., Kikuchi, M., Natsukawa, T., Shinobu, N., Imaizumi, T., Miyagishi, M., Taira, K., Akira, S., and Fujita, T. (2004). The RNA helicase RIG-I has an essential function in double-stranded RNA-induced innate antiviral responses. Nat. Immunol. *5*, 730–737.

Yount, J.S., Moran, T.M., and Lopez, C.B. (2007). Cytokine-independent upregulation of MDA5 in viral infection. J. Virol. *81*, 7316–7319.

Zevini, A., Olagnier, D., and Hiscott, J. (2017). Crosstalk between cytoplasmic RIG-I and STING sensing pathways. Trends Immunol. *38*, 194–205.

Zhou, X., Yang, J., Zhang, Z., Zhang, L., Zhu, B., Lie, L., Huang, Y., Ma, R., Zhou, C., Hu, S., et al. (2019). Different signaling pathways define different interferon-stimulated gene expression during mycobacteria infection in macrophages. Int. J. Mol. Sci. *20*, E663.

Zhu, J., Zhang, Y., Ghosh, A., Cuevas, R.A., Forero, A., Dhar, J., Ibsen, M.S., Schmid-Burgk, J.L., Schmidt, T., Ganapathiraju, M.K., et al. (2014). Antiviral activity of human OASL protein is mediated by enhancing signaling of the RIG-I RNA sensor. Immunity *40*, 936–948.

ISCI, Volume *22*

Supplemental Information

Cytoplasmic RNA Sensor Pathways and Nitazoxanide Broadly Inhibit Intracellular *Mycobacterium tuberculosis* Growth

Shahin Ranjbar, Viraga Haridas, Aya Nambu, Luke D. Jasenosky, Supriya Sadhukhan, Thomas S. Ebert, Veit Hornung, Gail H. Cassell, James V. Falvo, and Anne E. Goldfeld

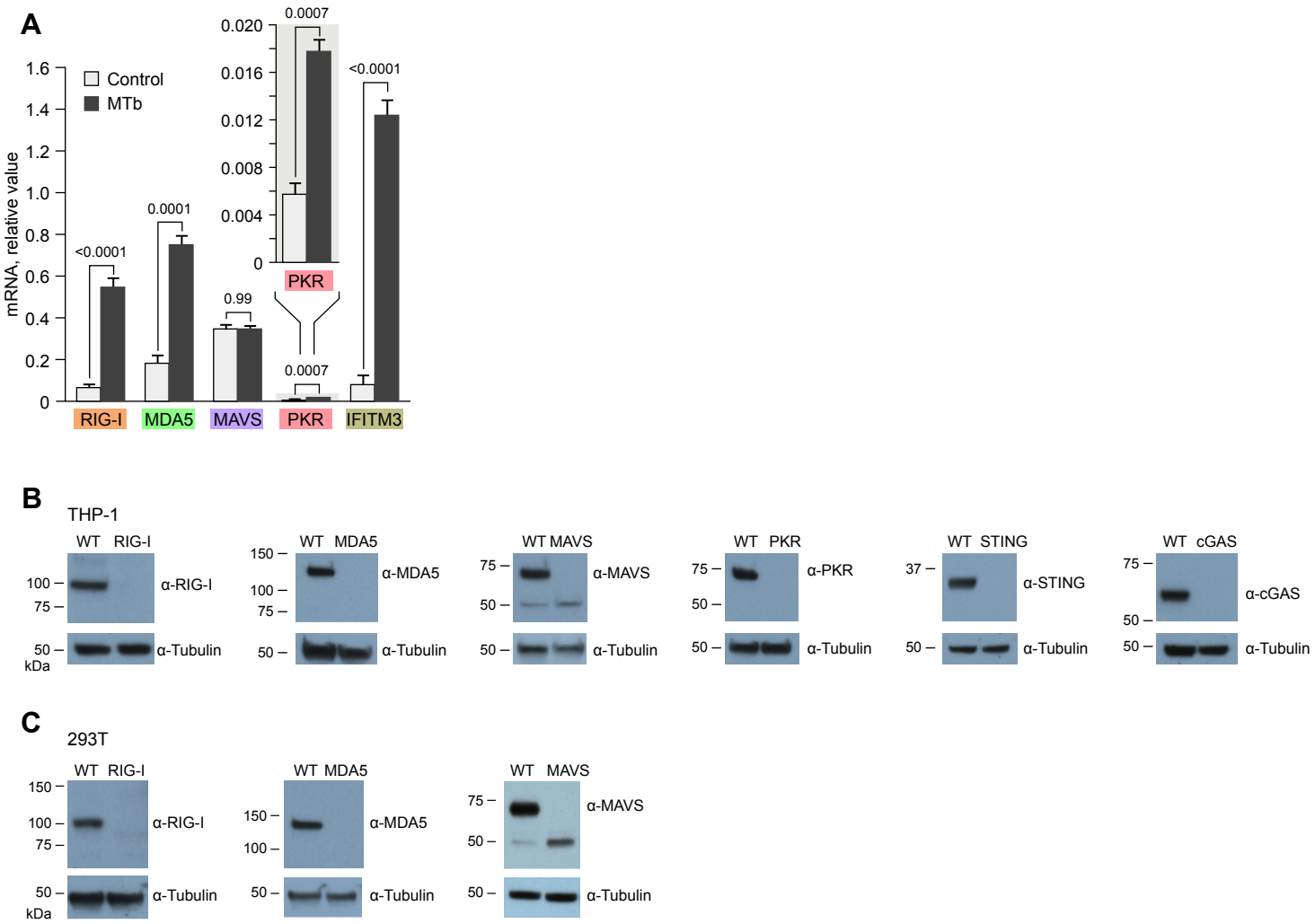

Supplemental Figure 1. MTb lysates induce RNA sensor RNAs and demonstration of disruption of RIG-I, MDA5, MAVS, PKR, STING, or cGAS by Western blot analysis of protein expression. Related to Figures 1 and 2. **A.** Stimulation of THP-1 cells with H37Rv whole cell lysates induces gene expression of cytosolic RNA sensing proteins. Related to Figure 1A. Gene expression in THP-1 cells that were mock stimulated or stimulated with MTb (H37Rv) lysates (30 µg /ml) for 3 or 24 hours as indicated using specific primers for RIG-I, MDA5, MAVS, PKR, and IFITM3 as described in Methods. After measurement by RT-PCR, results were normalized using cyclophilin B mRNA as an internal control and expressed as relative values of mRNA expression of RIG-I, MDA5, MAVS, PKR, or IFITM3. Data were analyzed using the unpaired Student's t-test and are presented as mean ± SEM of three independent experiments. **B.** Disruption of RIG-I, MDA5, MAVS, PKR, STING, or cGAS protein expression in THP-1 cells. Related to Figure 1B. Western blot analysis of control WT THP-1 cells or THP-1 cells where RIG-I, MDA5, MAVS, PKR, STING, or cGAS genes were disrupted as described in Methods. For the MDA5, MAVS, STING, or cGAS perturbed cells, which were created by Cas9/CRISPR, controls were a WT THP-1 cell line that was parental to the specific Cas9/CRISPR clone as done previously (Mankan et al., 2014; Paijo et al., 2016; Schmid-Burgk et al., 2014). The indicated antibodies, including tubulin as a control, were used to quantify the amount of protein in extracts from each cell line. **C.** Disruption of RIG-I, MDA5, or MAVS protein expression in 293T cells. Related to Figure 2B. Western blot analysis of wild type (WT) 293T cells or 293T cells where RIG-I, MDA5, or MAVS were ablated as described in Methods. The indicated antibodies, including an antibody to tubulin as a control, were used to quantify the amount of protein in extracts from each cell line.

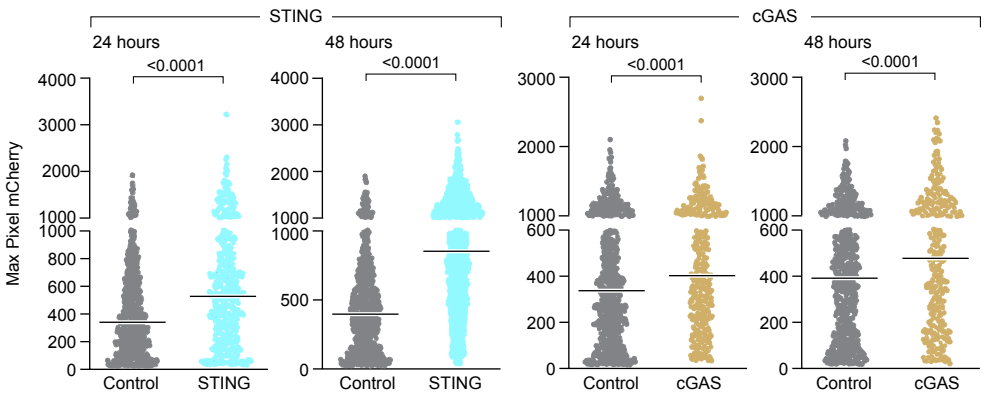

Supplemental Figure 2. Knockdown of STING or cGAS in THP-1 cells inhibits intracellular MTb growth. Related to Figure 1C. Quantitative IFC analysis of WT THP-1 control cells and cells in which STING or cGAS expression was disrupted (Fig. S1A) following infection with H37Rv-mCherry at 1:10 cell:bacilli for 24 hours or 48 hours as indicated. Dot plot graphs show the pixel intensity of intracellular mCherry in the infected cells. Data were analyzed using the Mann-Whitney Test and represents one of three independent experiments, acquiring ~5,000 cells per sample each time.

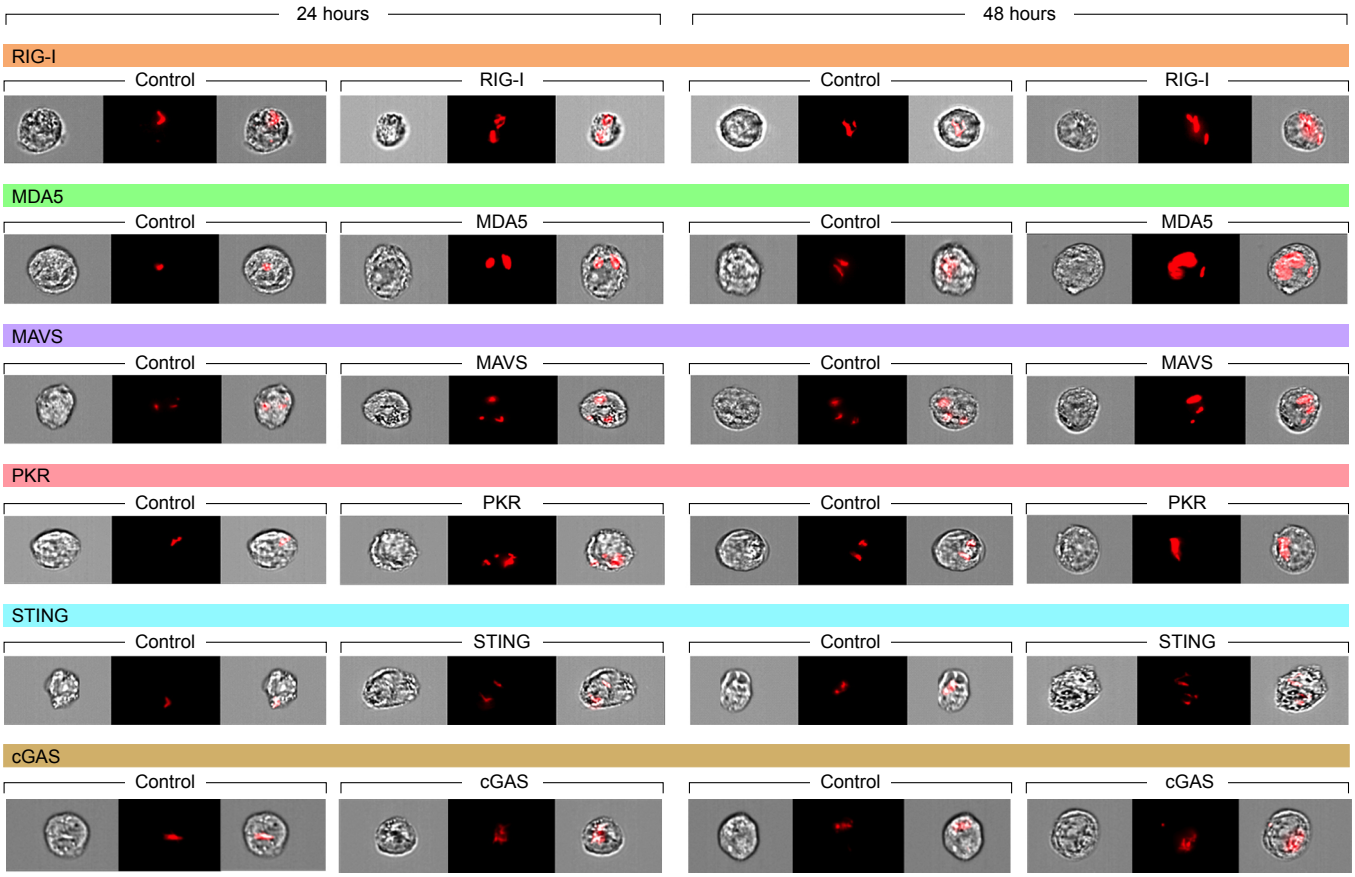

Supplemental Figure 3. Microscopy of MTb infection of WT and RIG-I-, MDA5-, MAVS-, PKR-, STING-, and cGAS-deficient THP-1 cells show intracellular MTb infection. Related to Figure 1C. Representative images are shown of individual THP-1 cells after ImageStream acquisition at median level of fluorescence intensity for each cell type and condition indicated. Bright-field microscopy (60x magnification) shows cells infected with MTb H37Rv-mCherry for 24 or 48 hours.

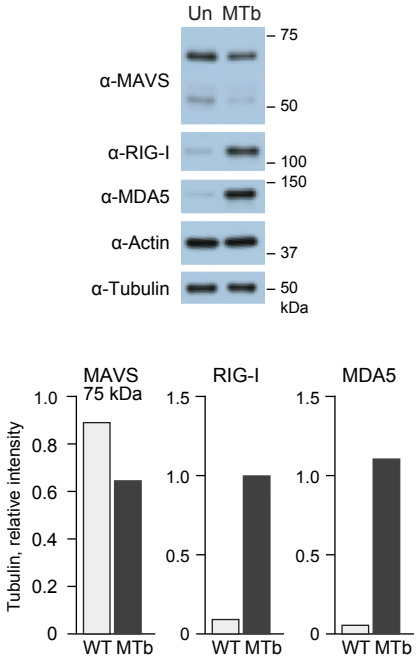

Supplemental Figure 4. MTb induction of RNA sensor protein levels parallels induction of RNA expression. Related to Figures1A. Western blot of MAVS, RIG-I, MDA5, actin, and tubulin protein expression in extracts from THP-1 cells uninfected (UN) or MTb infected for 24 hrs.

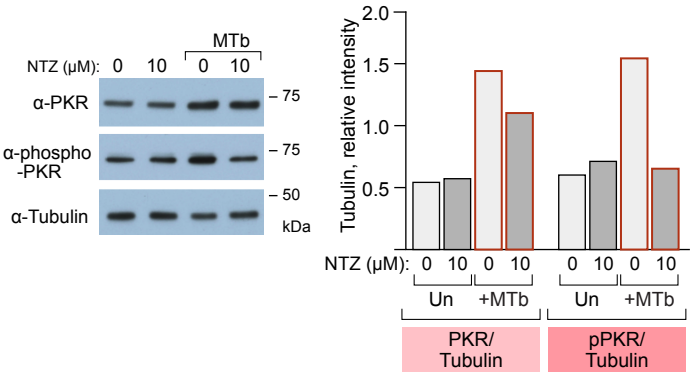

Supplemental Figure 5. MTb infection increases PKR and phosphorylated PKR protein levels while NTZ does not increase them. Related to Figure 3A. Left, Western blot of PKR, phosphorylated PKR, and tubulin (control) in extracts from THP-1 cells treated with vehicle or 10 μM NTZ and with or without MTb infection for 24 hrs. Right, plot of densitometric quantitation of PKR and phosphorylated PKR bands relative to tubulin bands from the blot.

TRANSPARENT METHODS

Ethics Statement: For isolation of peripheral blood mononuclear cells (PBMCs), we obtained unidentified, discarded leukocyte packs from the Boston Children's Hospital Blood Donor Center.

Cell Culture: Human PBMCs were isolated by Ficoll-Hypaque (Pharmacia) density gradient centrifugation. To prepare MDM, monocytes were enriched by positive selection with CD14 microbeads (STEMCELL Technologies) and then cultured at $1x10^6$ cells per well in six-well plates in RPMI-1640 medium with 2 mM L-glutamine (BioWhittaker), supplemented with 5% heat-inactivated human AB serum (Atlanta Biologicals) and 20 ng/ml recombinant human M-CSF (R&D Systems). After 5 days, supernatants were replaced with M-CSF-free medium prior to experimental analysis. More than 98% of the adherent cells obtained with this technique were $CD14^+$ macrophages, as verified by flow cytometry. The human monocytic cell line THP-1 was obtained from ATCC. PBMC or THP-1 cells were cultured in RPMI-1640 medium with 2 mM L-glutamine (BioWhittaker), supplemented with 10% FCS (Atlanta Biologicals). The human embryonic kidney cell line HEK-293T was obtained from ATCC and cultured in DMEM (BioWhittaker) supplemented with 10% FCS (Atlanta Biologicals).

Knockdown cell lines: 293T cells deficient for MAVS or DDX58 (RIG-I) (Yao et al., 2015; Zhu et al., 2014) were previously described. Briefly, a plasmid expressing a pair of zinc finger nucleases (ZFNs) designed to target exon 1 of RIG-I (Zhu et al.,

2014), or a pair of TALEN plasmids targeting MAVS (Yao et al., 2015) were transfected into 293T cells and single clones were validated by sequencing and Western blotting. THP-1 and 293T cells deficient for IFIH1 (MDA5) and THP-1 cells deficient for STING and cGAS were generated using CRISPR/Cas9 and single guide RNAs (sgRNAs). SgRNAs targeting an early coding exon of the indicated genes were designed. THP-1 cells were electroporated with pLK0.1-gRNA-CMV-GFP and CMV-mCherry-T2A-Cas9 expression plasmids using a Biorad GenePulser device as previously described (Schmid-Burgk et al., 2014). 293T cells were transiently transfected with the described plasmids using GeneJuice lipofection. mCherry positive cells were FACS-sorted and cloned by limiting dilution. Monoclones were duplicated and genotyped by deep sequencing (Illumina). Cell clones containing all-allelic frameshift mutations without wild-type reads were considered as knockout single-cell clones. The CRISPR/dCas9 PKR knockdown THP-1 cells were generated using a lentiviral vector encoding gRNA specific to the PKR gene promoter (or a gRNA directed to a scrambled nonsense sequence for control cells), dCas9-KRAB, and a puromycin resistance marker. Cells were selected with puromycin and PKR knockdown was analyzed by RT-qPCR as we described (Jasenosky et al., 2019). RIG-I deficient THP-1 cells and their corresponding control cell line were constructed as follows. Lentiviruses were produced by transfecting Lenti-XTM 293T cells (TaKaRa) with standard packaging vectors using TransIT-293 transfection reagent (Mirus) and filtering pooled supernatants through 0.45 μm PVDF filter followed by Lenti-X concentrator (TaKaRa). THP-1 cells were then lentivirally transduced with constructs expressing scrambled (Scr) sequence (pLKO.1 non-target shRNA,

SHC016) or DDX58 (RIG-I) (pLKO.1_TRC005, TRCN0000230212) shRNAs (Sigma) followed by puromycin selection.

Western Blot Analysis: Cells were cultured in DMEM or RPMI1640 complete media and used for Western blotting. Cell pellets were lysed in Laemmli buffer (62.5 mM Tris-HCl [pH 6.8], 2% sodium dodecyl sulfate, 2.5% β-mercaptoethanol, 10% glycerol, and 0.01% bromophenol blue; BIO-RAD) for 30 min in presence of protease inhibitors (Thermo Fisher Scientific), boiled for 5 min or 20 min (for all BL3 samples) at 100°C, and subjected to Western blot analysis. Primary antibodies: DDX58 (RIG-I) (1:2,000, D14G6, 3743, Cell Signaling Technology (CST)), IFIH1 (MDA5) (1:2000, D74E4, 5321, CST), EIF2AK2 (PKR) (1:5,000, Y117, ab32506, Abcam), MAVS (1:2000, polyclonal, 3993, CST), TMEM173 (STING) (1:2000, D2P2F, 13647, CST), phospho-EIF2AK2 (PKR phosphorylated at Thr451) (1:2000, polyclonal, 07-886, Millipore), CGAS (cGAS) (1:2000, D1D3G, 15102, CST) and TUBA4A (α-tubulin) (1:5,000, B-5-1-2, T5168, SIGMA). Blots were probed with anti-mouse (1:2,000, 7076, CST) or anti-rabbit (1:2,000, 7074, CST) IgG-HRP secondary antibody and visualized using SuperSignal West Pico PLUS Chemiluminescent Substrate (Thermo Fisher Scientific) or SuperSignal West Femto Maximum Sensitivity Substrate (Thermo Fisher Scientific).

Expression plasmids and cell stimulation: The pFLAG-CMV4 vectors encoding full-length RIG-I, MDA5, or MAVS have been described previously (Wu et al., 2014) and pFLAG-CMV4 was used as an empty vector control. Cells were transfected with

these vectors using lipofactamine2000 (Invitrogen), incubated 18 hours, and infected with MTb for 24 hours, in the presence or absence of NTZ (a gift from Romark) for 4 hours prior to infection as indicated after which the cultures were terminated and total RNA was extracted, as previously described (Ranjbar et al., 2015). For the RNA analysis of RNA and DNA sensor responsiveness, THP-1 cell lines in which PKR, RIG-I, MDA5, or MAVS were knocked down or control cells (1×10^7) were bulk differentiated by overnight incubation in 100 ng/mL PMA in 10 cm dishes. Cells were washed twice with PBS and detached using trypsinization. 5×10^5 cells were seeded per 48-well plate in RPMI-1640 medium with 2 mM L-glutamine, supplemented with 10% FCS overnight, after which the differentiated cells were transfected with 400 ng of 5'ppp dsRNA (InvivoGen), high molecular weight (average size 1.5-8 kb) poly I:C (InvivoGen), or herring sperm DNA (Sigma), or mock transfected, using Lipofectamine2000 (Invitrogen). Cultures were further incubated at 37°C and 5% CO_2 for 8 hours, after which they were terminated and total RNA was extracted for further analysis. In the case of MTb whole cell lysates (H37Rv) (BEI Resources) (NR-14822), 30 μg/ml were used to stimulate THP-1 cells as indicated.

MTb Culture: The MTb strains H37Rv and H37Rv-mCherry (kindly provided by Dr. Sarah Fortune; (Sillé et al., 2011)) were prepared as described previously (Ranjbar et al., 2009). Bacteria were grown in Middlebrook 7H9 medium (Difco BD, Franklin Lakes, NJ) supplemented with albumin dextrose complex (ADC) and 0.05% Tween 80 (Sigma-Aldrich, Saint Louis, MO). Bacteria were grown to an OD_{650} of 0.4 at 37°C,

which assured that they were in logarithmic growth phase. Cells were then pelleted and washed with PBS, re-suspended in PBS, and passed through a 5 μm filter to ensure that the bacteria were in a single cell suspension. Bacterial cell numbers were determined by measurement of OD_{650} before further dilution for cell infection studies.

Cellular stimulation and analysis by quantitative PCR: MDM, THP-1, and 293T cells were infected with H37Rv at a ratio of 1 or 10 bacteria per 1 cell as previously described (Ranjbar et al., 2015) in the presence or absence of NTZ as indicated, and mRNA expression levels were determined by SYBR Green-based real-time PCR (Bio-Rad Laboratories) as described previously (Ranjbar et al., 2015) with the following gene-specific primers: IFITM3 (forward, 5'-GCTGATCTTCCAGGCCTATG-3'; reverse, 5'-GATACAGGACTCGGCTCCGG-3'); IFN-β (forward, 5'-GAATGGGAGGCTTGAATACTGCCT-3'; reverse, 5'-TAGCAAAGATGTTCTGGAGCATCTC-3'); PKR (forward, 5'-GGCACCCAGATTTGACCTTC-3'; reverse, 5'-TCCTTGTTCGCTTTCCATCA-3'); RIG-I (forward, 5'-GAAGACCCTGGACCCTACCTA-3'; reverse, 5'-CCATTGGGCCCTTGTTGTTT-3'); MDA5 (forward, 5'-CTCAGGCCTTACCAAATGGA-3'; reverse, 5'-TCCAGGCTCAGATGCTTTTT-3'); MAVS (forward, 5'-CCTAAGGCCCTCTCTTTGCT-3'; reverse, 5'-GCACCTCCAAAGAGCTTGAC-3'); and Cyclophilin B (PPIB) (forward, 5'-AGAAGAAGGGGCCCAAAG-3' ; reverse, 5'-AAAGATCACCCGGCCTACA-3'). The reaction conditions were 95°C for 10 min followed by 40 cycles of 95°C for 15 sec and 60°C for 1 min. The results were

normalized using cyclophilin B mRNA as an internal control and expressed as relative values.

CFU Assay: Normal donor PBMC (2 x 10^6) were seeded in twelve-well plates in triplicate and were treated with 10 μM of NTZ, TIZ, RM5061 (gifts from Romark) or DMSO as control for 4 hours, after which they were infected with H37Rv (cell:bacteria, 1:10). After a 4-hour incubation at 37°C and 5% CO_2, the cultures were treated with 50 μg/ml puromycin for 20 min. Cells were washed three times with PBS; cultured in 3 ml fresh RPMI medium plus 10% FCS without or with 10 uM NTZ, TIZ, or RM5061; and incubated at 37°C and 5% CO_2. Following each time point, cultures were terminated, cells were treated with lysis buffer and sonicated, and serial dilutions were prepared and inoculated in Middlebrook 7H11 agar in triplicate. Colonies were counted on day 25 post-infection. THP-1 cell lines (1.5 x 10^6) were seeded in twelve-well plates in triplicate and infected with H37Rv (cell: bacteria, 1:10) and then treated as described above. The same procedure of CFU analysis was performed in the THP-1 control and RNA sensor perturbed cells lines infected with MTb.

Flow Cytometry: For standard cytometric analyses, cells were left uninfected or infected with MTb-mCherry for the indicated time points, after which the cultures were terminated. Cells were washed with PBS, fixed with 4% paraformaldehyde, and analyzed with a five-laser FACSAria SORP machine (Becton Dickinson) according to standard techniques. Results were analyzed using the FlowJo software package.

ImageStream analysis: Cells were infected with MTb H37Rv-mCherry for the indicated time points and treated with NTZ (a gift from Romark) as described above for 4 hours prior to or after infection as indicated. Cultures were terminated and cells were fixed with 4% paraformaldehyde. ~5,000 cells per sample were acquired using an Amnis ImageStreamX Mark II machine (EMD Millipore), with simultaneous collection of bright field, fluorescence, and scatter of images on a per-cell basis. Objective numerical quantification of internalized H37Rv-mCherry was performed using IDEAS software (Haridas et al., 2017).

Statistical Analysis: Where applicable, results are expressed as mean ± SEM. Comparison between two groups was performed using the unpaired Student's t-test with the aid of Microsoft Excel software or the Mann-Whitney Test using Graph-pad Prism software. A p value of 0.05 was considered significant.

SUPPLEMENTAL REFERENCE

Ranjbar, S., Boshoff, H.I., Mulder, A., Siddiqi, N., Rubin, E.J., and Goldfeld, A.E. (2009). HIV-1 replication is differentially regulated by distinct clinical strains of *Mycobacterium tuberculosis*. PLoS One *4*, e6116.